Journal of Materials Chemistry B

ROYAL SOCIETY OF CHEMISTRY

REVIEW

View Article Online
View Journal | View Issue

Cite this: J. Mater. Chem. B, 2025, 13, 454

Recent advances in polymer-based thin-film electrodes for ECoG applications

Zhengchen Xiang,[a] Liangtao Yang,*[b] Bin Yu,*[a] Qi Zeng,[b] Tao Huang,[a] Shuo Shi,[c] Hao Yu,[a] Yi Zhang,*[b] Jinglong Wu[b] and Meifang Zhu[a]

Received 18th September 2024,
Accepted 10th November 2024

DOI: 10.1039/d4tb02090a

rsc.li/materials-b

Electrocorticography (ECoG) has garnered widespread attention owing to its superior signal resolution compared to conventional electroencephalogram (EEG). While ECoG signal acquisition entails invasiveness, the invasive rigid electrode used inevitably inflicts damage on brain tissue. Polymer electrodes that combine conductivity and transparency have garnered great interest because they not only facilitate high-quality signal acquisition but also provide additional insights while preserving the health of the brain, positioning them as the future frontier in the brain–computer interface (BCI). This review summarizes the multifaceted functions of polymers in ECoG thin-film electrodes for the BCI. We present the abilities of sensitive and structural polymers focusing on impedance reduction, signal quality improvement, good flexibility, and transparency. Typically, two sensitive polymers and four structural polymers are analyzed in detail in terms of ECoG electrode properties. Moreover, the underlying mechanism of polymer-based electrodes in signal quality enhancement is revealed. Finally, the remaining challenges and perspectives are discussed.

1. Introduction

The brain–computer interface (BCI) is the technology that transmits biopotential signals generated by stimulating neurons in the brain to external electronic devices, enabling artificial control and intervention.[1–3] Electrocorticography (ECoG) uses thin film electrodes that are placed on the surface of the brain, resulting in higher electrical signal intensity than electroencephalogram (EEG), which is recorded on the scalp noninvasively. Both of them are highly suitable for BCI application to monitor health status.[4–7] Additionally, the BCI has been employed for drug delivery[8,9] through the implantation of microchannel electrodes, offering treatments for neurological disorders, such as epilepsy, Alzheimer's disease, and Parkinson's disease.[10] These advances in BCI technology possess great promise for neural healthcare management and artificial intelligence.[11]

To meet the demands of BCI development, it is crucial to record stable and high-quality biopotential signals, which has led to increased attention on electrodes.[12,13] Electrodes used for brain potential recording can be categorized into non-invasive, semi-invasive, and invasive electrodes. Non-invasive electrodes are always used to monitor brain alpha and beta rhythms (0–40 Hz) through external monitoring, completely avoiding interference with brain tissue. Performance distinctions among three different types of electrodes exhibiting varying degrees of invasiveness are outlined in Table 1, and the differentiation between these diverse signals is listed in Table 2.[14] However, non-invasive electrodes are strongly affected by the skull, and their signal quality may not meet the requirements for deeper-level research. Invasive electrodes

Table 1 Comparison of three different types of electrodes in skull filtration, craniotomy, and nerve injury

Type	Skull filtration	Craniotomy	Nerve injury	Ref.
Non-invasive	Yes	None	None	26
Semi-invasive	No	Craniotomy	None	25
Invasive	No	Craniotomy	Nerve injury	27 and 28

Table 2 Neural signal comparison[14]

Sign	Frequency	Amplitude	Rhythm	Stability
EEG	0.5–100 Hz	5–300 μV	Slow rhythms	Decades
ECoG	<200 Hz	0.01–5 mV	Medium rhythms	Decades
LFP	<200 Hz	0.01–1 mV	—	Year
AP	0.1–7 kHz	500 μV	—	Month

[a] State Key Laboratory for Modification of Chemical Fibers and Polymer Materials, College of Materials Science and Engineering, Donghua University, Shanghai 201620, China. E-mail: yubin@dhu.edu.cn
[b] Research Center for Medical Artificial Intelligence, Shenzhen Institute of Advanced Technology, Chinese Academy of Sciences, 518055 Shenzhen, China. E-mail: liangtao.yang@siat.ac.cn, yi.zhang3@siat.ac.cn
[c] School of Fashion and Textiles, The Hong Kong Polytechnic University, 999077, Hong Kong S.A.R, China

penetrate the brain to obtain high-resolution biopotential signals, such as local field potential (LFP) and action potential (AP). However, invasive electrodes are made of rigid materials such as steel, which is not flexible in brain tissue.[15] This leads to tissue damage during experiments, limiting subject mobility. Moreover, long-term implantation of probes leads to the accumulation of glial sheaths around the probe,[1,16–20] reducing the electrode's stability.[21,22] Semi-invasive electrodes, especially ECoG electrodes, primarily consist of a two-dimensional thin-film. These thin-film electrodes are typically placed under the hard meninges on the surface of the cerebral cortex and can record ECoG signals with high bandwidth and low noise.[23] These collected good signals contribute to the study of the BCI. Due to the good elastic properties of thin-film materials, electrode implantation causes minimal interference to brain tissues, making it a subject of interest. In recent years, research on semi-invasive electrodes has attracted great attention.[24,25] The recent development of ECoG thin-film electrodes is shown in Fig. 1.

The configuration of semi-invasive electrodes requires good shape contact with the brain. However, traditional ECoG electrodes, due to the rigidity of silicon-based substrates and metal conductors, do not match the mechanical properties of the soft brain tissue, making them prone to damage.[36] Polymer materials provide an excellent solution to avoid this mechanical mismatch. Conventional polymer materials, such as polydimethylsiloxane (PDMS),[31,37–43] polyimide (PI)[44] and parylene[31,32,38,40,43,45–55] have a low Young's modulus. Some studies have achieved high tensile strength and good transparency using a combination of two polymer films. This opens up possibilities for further applications of ECoG electrodes in optogenetics, providing the potential for external control of the brain. PI can be used to form flexible films for circuit integration and active electronic devices through spin coating and electrospinning.[56,57] Liquid crystal polymers (LCP) have also received more attention due to their excellent biocompatibility.[58–60] Furthermore, to improve the conformal contact between the electrode and brain tissue, conductive polymers are typically coated on the surface of a metal layer. These polymer materials reduce the contact impedance between the electrode and the skin interface due to their good conductivity and flexibility compared to metal materials. Poly(3,4-ethylenedioxythiophene):poly(styrene sulfonate) (PEDOT:PSS) has high transparency and good conductivity, and these properties make this material widely used in the preparation of electrophysiological electrodes. Sergio *et al.* introduced PEDOT:PSS into Pt electrodes by electroplating, leading to a lower electrochemical impedance by approximately 30 times (from 971 007 Ω to 30 407.6 Ω) at 1 kHz compared to the bare Pt electrode. Polymers can significantly improve the signal quality of ECoG, and they have become one of the most critical electrode components for brain biopotential recording.

With the growing interest in BCI, more and more articles are being published on understanding this interdisciplinary field.[11] In terms of engineering, there is a focus on achieving more extensive and long-term recordings.[61] These reports focused on the development, prospects, and application scenarios of BCIs.[62] In terms of material science, conductive materials such as silicon-based materials,[63] fiber materials,[64] conjugated polymer materials,[65] and semiconductor polymer materials[66] have been reviewed and discussed. However, in most of these reviews, the electrodes were introduced only based on their physicochemical properties. There is still a lack

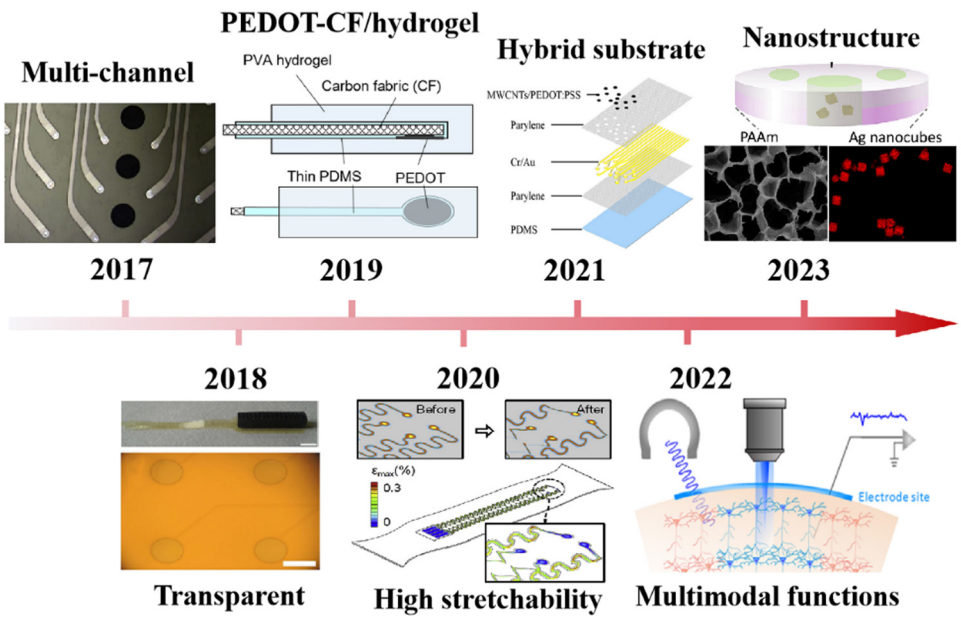

Fig. 1 (a) Development of ECoG thin-film electrodes. Reprinted with permission from ref. 29. Copyright 2023, American Chemical Society. Reprinted with permission from ref. 30. Copyright 2022, Elsevier. Reprinted with permission from ref. 31. Copyright 2021, American Chemical Society. Reprinted with permission from ref. 32. Copyright 2020, Journal of Materiomics. Reprinted with permission from ref. 33. Copyright 2019, Scientific Reports. Reprinted with permission from ref. 34. Copyright 2018, Elsevier. Reprinted with permission from ref. 35. Copyright 2017, Elsevier.

of comprehensive discussion about the correlation between the structure, properties and signal performance.

In this work, the electrode performance was classified based on the detection requirements of ECoG signals, including electrical, mechanical, and optical properties. The criteria to be considered mainly include electrode-skin impedance, Young's modulus, and transparency, which are summarized. According to our investigation, the addition of polymer materials has brought improvements to ECoG thin-film electrodes in terms of conductivity and flexibility, demonstrating the potential for enhancing the electrode signal quality. In order to distinguish these polymer materials, they are divided into two categories based on their contribution to electrode properties. The first is sensitive materials, like PEDOT and PPy, which are in contact with the skin because of their high conductivity. The second type, structure materials, such as polydimethylsiloxane, parylene, polyimide, liquid crystal polymer *etc.*, have been commonly used in the substrate and insulation layer of ECoG thin-film electrodes. The available electrode preparation methods and relevant properties are discussed. Finally, the challenges and perspectives of polymer-based ECoG thin-film electrodes are also discussed.

2. Characteristics of polymer materials

ECoG thin-film electrodes are divided into two parts: sensitive materials and structural materials. The sensitive materials provide the electrical properties required for the electrodes, while the structural materials like the substrate, insulation layer and sacrificial layer provide the mechanical and optical properties required for the electrodes, such as structural support, adhesion of metals, and improvement of transmittance.[12]

The electrode materials and thin-film materials for ECoG thin-film electrodes are compared in Table 3. The performance of electrodes with different materials, including sensitive materials of Ti, Au, Cr, Pt, indium tin oxide (ITO), poly(3,4-ethylenedioxythiophene)-modified carbon fabric (PEDOT-CF), PEDOT:PSS, multiwalled carbon nanotubes (MWCNTs), and structure materials of polyvinyl alcohol (PVA), PDMS, PI, and polyethylene glycol terephthalate (PET) are listed.

2.1 Electrical properties

Acquiring ECoG signals necessitates electrode materials possessing favorable electrical characteristics. For polymer materials, conductive polymers (CPs)[76] with lower impedance are often used for electrodes. These CPs encompass organic polymeric conductors, such as PEDOT, polypyrrole (PPy), and polyaniline (PANI).[77,78] PPy is a biocompatible substance extensively employed in biomedical scenarios, and it can be synthesized *via* chemical oxidation, electrochemical oxidation, and photopolymerization methods.[79] PANI offers the advantages of cost-effectiveness and ease of synthesis. Nevertheless, the primary polymer chain's rigidity renders engaging in machining operations.[80,81] PEDOT exhibits the advantages of good suppleness, high transparency, and good conductivity.[82] Incorporating PSS

Table 3 The materials and properties of the ECoG thin-film electrodes

	Sensitive materials	Structural materials	Property	Ref.
1	Ti/Au	Parylene C and PDMS	Bending cycle reaches 200 000 times impedance is 12.65 kΩ at 1 kHz charge storage capacity is 207.5 μC cm^{-2}	38
2	Ti/Au	Parylene C	Impedance is 10^4 Ω level at 1 kHz long-term recording stability	51
3	Au	PI	Impedance is 10^7 Ω level at 1 kHz max strain less than 0.03% at 3.8 mm bending radius	67
4	Au	PI	Impedance is 1.1 ± 1.2 kΩ at 1 kHz	68
5	Au	Parylene and PDMS	Impedance between 50 and 70 kΩ at 1 kHz	48
6	Pt	OSTEMER 324 Flex	Surface curvature adapts to the brain	69
7	Cr/Au	BPDA-PD PI	Waterproofness	70
8	Cr/Au/Pt	Parylene C	Transparent	47
9	Pt	PI 2611	Impedance is 10^2 Ω level at 1 kHz	25
10	Glassy carbon	PI	Impedance is 10^4 Ω level at 1 kHz (300 μm)	71
11	Glassy carbon	PI	Impedance is 10^4 Ω level at 1 kHz long-term recording stability	72
12	ITO	Parylene C and PDMS	Transparent	52
13	ITO	PI	Transparent	34
14	ITO	Parylene HT	Transparent	50
15	Carbon nanotube array	PDMS	Transparent extracellular ion monitoring	41
16	PEDOT-CF	PVA hydrogel and PDMS	Shape adaptability double layer capacitance is 70 mF cm^{-2}	33
17	PEDOT:Nafion coated gold	PI	$\|Z\|$ values are about 100 kΩ at 1 kHz	73
18	PEDOT:PSS–ITO–Ag–ITO	Parylene C	Young's modulus is about 4.064 GPa the resistivity of the average thin layer resistance is 7.40×10^{-5} Ω cm transparent	49
19	(MWCNTs)/PEDOT:PSS	PDMS–parylene hybrid	Average impedance is 20.2 ± 7.9 kΩ at 1 kHz transparent	31
20	Silver and PEDOT:PSS	PET and parylene	Impedance is 81.4 ± 53.4 kΩ at 1 kHz transparent	74
21	Cr/Au/Ti coated PEDOT-CNT	PI	Impedance is 10^3 Ω level at 1 kHz	75
22	PEDOT:PSS coated Pt/Au/Pt	Parylene C and PDMS	Impedance is 30.4 ± 2.4 kΩ at 1 kHz transparent	43

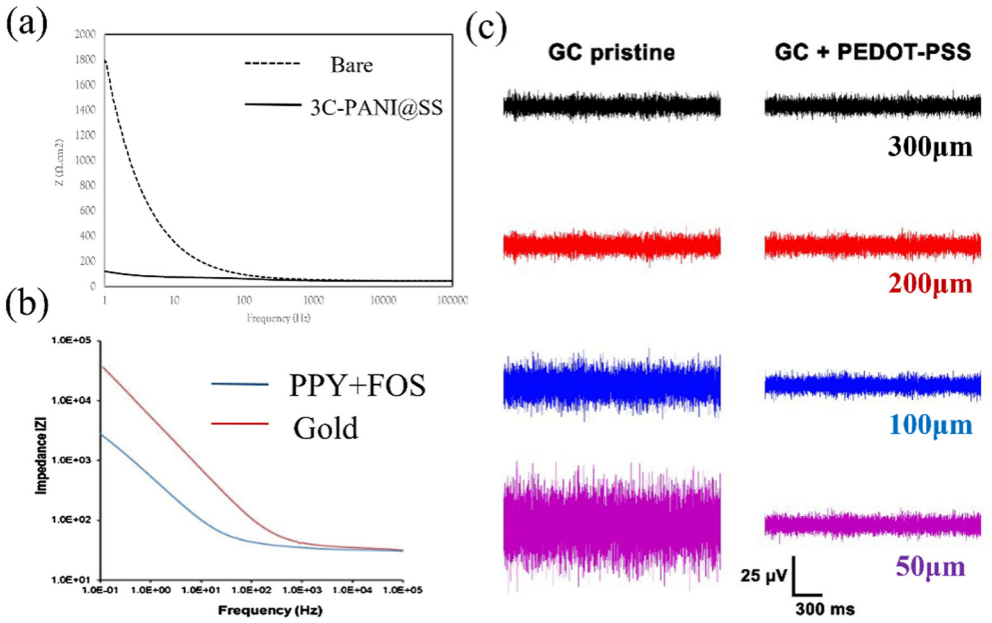

Fig. 2 (a) The contact impedance between the PANI-coated electrode and bare electrode. Reprinted with permission from ref. 85. Copyright 2021, Elsevier. (b) Impedance diagram between the PPy coated electrode and bare electrode. Reprinted with permission from ref. 8. Copyright 2016, Elsevier. (c) The electrode noise effects of GC electrodes having different areas with PEDOT:PSS. Reprinted with permission from ref. 71. Copyright 2018, MDPI.

into PEDOT yields water-soluble PEDOT:PSS, thereby enhancing its processing performance.[83,84]

CPs can be modified onto the electrode surface *via* coating or electroplating methods, with the intention of mitigating electrode impedance. Sergio *et al.* employed electroplating to coat PEDOT:PSS onto the Pt electrode, reducing the electrochemical impedance by 30 fold.[43] Fig. 2a illustrates the contact impedance of PANI-coated electrodes and bare electrodes. The PANI coating leads to a reduction in electrode contact impedance ($Z = 120\ \Omega\ cm^2$ *vs.* $Z = 1808\ \Omega\ cm^2$).[85] Similarly, the same trend is observed with PPy coating. Rikky *et al.* compared the impedance of PPy + FOS (blue) with those of gold (red), unveiling a decrease in electrode impedance following PPy coating (Fig. 2b).[8] Saeed *et al.* enhanced the conductivity from 10^{-4} to 10^{-2} by introducing oligoaniline into the composition.[86] Yang *et al.* designed and added PEDOT:PSS on the surface of the ITO-Ag-ITO structure, which greatly reduced the electrode impedance.[49] Moreover, the PEDOT:PSS coating further decreases the impedance. Castagnola *et al.* showed that the impedance of the gold-CNT-coated electrode impedance diminished by two-thirds compared to the bare sample, and the PEDOT-CNT-coated electrode achieved a two-order decrease in impedance at 100 Hz compared to the uncoated electrode.[87] Moreover, the electrical performance of the electrode is related to its size; as the electrode diameter decreases, the background noise within the acquired signal exhibits a concurrent rise (Fig. 2c). However, small-sized ECoG electrodes are crucial for conducting experiments, and maintaining better electrical properties of ECoG electrodes at small sizes has become a challenge. Enhancing the electrical conductivity of materials offers a means to reduce the background noise.[71] Following the application of PEDOT:PSS coating onto a glassy carbon (GC) electrode with a 50 μm thickness, a background noise intensity similar to a 300 μm diameter electrode can be achieved. This consequently mitigates the noise stemming from the reduction in electrode area.

2.2 Mechanical properties

The mechanical properties of the electrode are determined by its Young's modulus.[88,89] Polymer materials are similar to brain tissues in terms of Young's modulus, distinguishing them from metal and non-metallic carbon-based materials (Fig. 3). The reported flexible substrate materials for electrodes include PI, PDMS, parylene, and LCP. These materials enable the electrode to achieve good flexibility and stretchability, resulting in

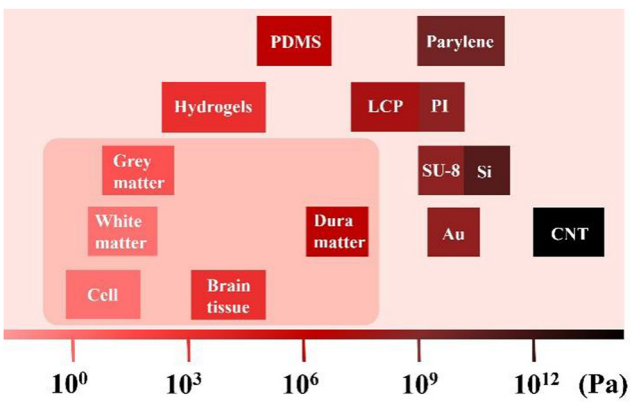

Fig. 3 The Young's modulus of various materials, cells and brain tissues (scale bar). Data derived from ref. 1, 30, 42 and 58.

improved comfort and good contact with the skin and underlying tissue. As a result of this increased flexibility, the electrode achieves improved accuracy and stability in acquiring ECoG signals.

Wu *et al.* mentioned that the modulus of the brain tissue is about 100 KPa, and that of the implantable Si electrode is about 150 GPa; this big mismatch will cause mechanical trauma, resulting in acute inflammation. They also measured the modulus of hydrogels: ~100 kPa, Au: ~80 GPa, and CNT: ~1 TPa. Wang *et al.* reported that the modulus of white matter and grey matter is about 300 Pa and 450 Pa, and dura mater is about 1 MPa. Guo *et al.* calculated the Young's modulus of different soft film materials (PDMS: ~1 MPa, PI: ~2.8 GPa, parylene: ~4.5 GPa, SU-8: ~5.6 GPa). Yang *et al.* claimed that the modulus of LCP is from MPa to GPa levels. From the perspective of mechanical properties, hydrogel seems to be the most suitable material, but it is seriously affected by the moisture conditions and has high requirements for the use environment.

In many cases, PDMS and LCP emerge as more flexible options for a wide range of microfluidic applications and biomedical devices. Their flexibility and biocompatibility render them preferable choices. Conversely, in settings necessitating printed circuits or stringent conditions, PI stands out as an excellent option due to its high-temperature stability and chemical inertness, enabling optimal performance even under extreme circumstances. Moreover, parylene demonstrates proficiency in bonding with sensitive materials. Its highly uniform coating and good chemical inertness establish it as a frequently utilized protective coating in both biomedical and electronic devices.

2.3 Optical properties

In contrast to many metal and inorganic non-metallic counterparts, polymer materials typically exhibit superior light transmittance. This is beneficial for stimulating the brain with light to achieve disease treatment. The schematic diagram of light stimulation is shown in Fig. 4a. Fig. 4b shows an ECoG thin-film electrode made of various polymer materials, which has good transparency.[30] For example, optogenetics affords targeted neuronal manipulation with millisecond precision,[90] enabling the potential artificial regulation of brain nerve excitation through light stimulation for addressing neurodegenerative disorders, *i.e.*, Parkinson's disease, epilepsy, and depression.[91] Facilitated by highly light-transmissive ECoG electrodes, researchers employed optogenetics to modulate channel protein activity within the mouse brain, thus controlling nerve excitation and inhibition. Therefore, in recent years,

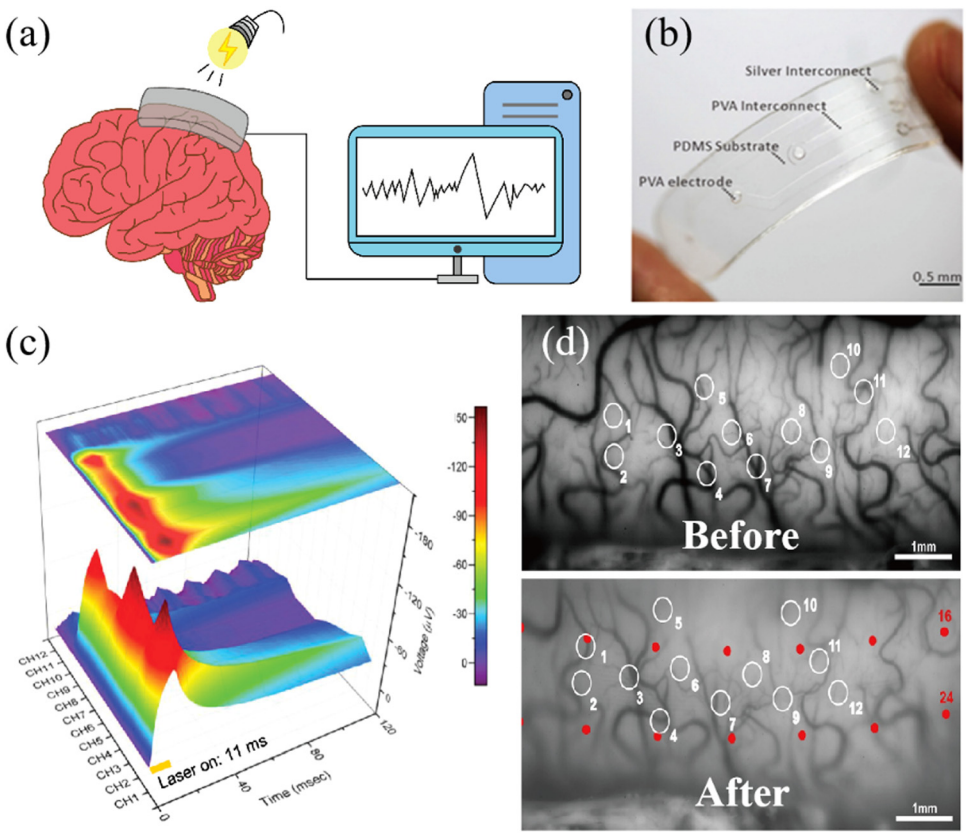

Fig. 4 (a) The transparent ECoG thin-film electrode composed of multiple polymers. (b) Schematic of ECoG signal stimulated by light. Reprinted with permission from ref. 30. Copyright 2022, Elsevier. (c) The ECoG signal induced by continuous stimulation of the cerebral cortex of the marmoset by a blue laser pulse through a transparent electrode for 11 milliseconds. Reprinted with permission from ref. 93. Copyright 2019, WILEY. (d) Vascular images of cat visual cortex A18 before and after the installation of the ECoG thin-film electrode. Reprinted with permission from ref. 34. Copyright 2018, Elsevier.

there has been growing research on the application of transparent polymer materials in ECoG electrodes.[92]

Concerning optical properties, glass is commonly used as an inorganic transparent material for comparison, and indium-doped tin oxide (ITO) constitutes a commonly used transparent thin-film material.[94] Yang *et al.* compared the transmittance between ITO and PEDOT:PSS-ITO-Ag-ITO multilayer films on glass and parylene C substrates. They noted an increase in transmittance on parylene C substrates from 78% (ITO) to 85% (multilayered film). Similarly, on glass substrates, the transmittance rises from roughly 75% (ITO) to about 89% (multilayered film). The study validated that the parylene C multilayered film achieves transmittance at wavelengths of 470 nm, 550 nm, and 630 nm.[46] Similarly, the electrode coated with PEDOT: PSS by Yang *et al.* showed stable signal-to-noise ratio (SNR) under different wavelengths of light conditions, with a variation of less than 2.7% and an average signal-to-noise ratio range of 35 db to 36 db. With the successful preparation of transmittance ECoG electrodes for more wavelengths of light, more choices can be obtained from light therapy to light stimulation.[47] Similarly, changes in the intensity of ECoG signals can also be used to detect the health status of the brain. Fig. 4c displays the ECoG signals obtained by stimulating the marmoset brain with blue light. These signals were recorded using a 12-channel electrode. When the brain is affected by a virus, a high response is obtained through blue light stimulation, corresponding to the highest peak values of 150 μV in channels 1, 5, and 9 in Fig. 4c, which correspond to the virus-infected area. This method of detecting signals through transparent electrodes to obtain health status is very useful for medical diagnosis.[49] Of course, it is important to note that the duration of light stimulation and irradiance levels will also impact the photogenetically evoked potential, as they directly influence the activation and response of photosensitive cells or molecules, thus affecting the magnitude and duration of the elicited neural activity.

3. Polymers for ECoG thin-film electrodes

In the following section, the materials are categorized as sensitive materials and structure materials. For each specific material, we will first introduce their preparation methods, followed by their properties.

3.1. Sensitive materials

Conductive polymers (CPs) predominantly derive their structure from a sequence of alternating single and double bonds. This conjugated arrangement facilitates the facile movement of electrons within and between polymer chains, thereby elevating the conductivity of polymer materials.[9] Notable instances include PANI,[85,86] PPy[95] and PEDOT.[2,31,33,39,43,46,49,68,71,74,75,87,96–99] CPs typically exhibit flexibility, conductivity, biocompatibility, and facile processing at ambient temperatures. The techniques employed for depositing CPs onto electrodes primarily involve spin coating and electropolymerization.[100] While spin coating technology is relatively straightforward, it is unsuitable for application on small, non-planar surfaces. In contrast, the electro-polymerization method proves to be a more precise approach for applying CPs to surfaces that are incompatible with spin coating techniques.[97,101] For thin-film electrodes used in ECoG, the prevailing choice of CPs materials predominantly centers around PEDOT and PPy.[75,96,97]

3.1.1. Poly(3,4-ethylenedioxythiophene). PEDOT is synthesized from the monomer EDOT through chemical oxidation and electrochemical polymerization.[83,102,103] It boasts attributes such as a narrow bandgap, chemical stability, and charge mobility.[104] Typically, PEDOT is combined with acidic PSS[105] to form PEDOT:PSS, a conductive polymer that exhibits conductivity and transparency. The resultant conductive polymer PEDOT:PSS is a printable conductor.[74] Furthermore, it demonstrates superior impedance characteristics compared to conventional metal electrodes, especially within the frequency range of brainwave activity (0.1–1000 Hz). Due to its good chemical stability and biocompatibility, PEDOT:PSS is highly suitable for long-term implanted ECoG thin-film electrodes.

In terms of structure, the electrode employs electropolymerization to prepare a PEDOT layer at the base of the carbon fabric (CF) electrode in an effective way, as displayed in Fig. 5a.[33] The reverse side of the electrode and the lead are insulated through a thin PDMS coating, while the outer layer is treated with a PVA hydrogel. This design ensures the electrode maintains conductivity while retaining flexibility equivalent to living tissues. Carbon nanotubes (CNTs) exhibit mechanical strength and electrical properties. The amalgamation of carbon nanotubes with PEDOT, leading to PEDOT-CNTs, enhances conductivity[106–108] and stability and augments adhesion to the electrode surface. For instance, the nanocomposite electrode created by multiwalled carbon nanotubes (MWCNTs) in conjunction with PEDOT:PSS yields a rugged and porous surface *via* a network of interwoven nanostructures, as depicted in Fig. 5b.[31] This configuration increases the electrochemical surface area and elevates electrode conductivity. Although high conductivity has been achieved, a stable testing *in vivo* environment is still lacking. The transparent electrode made by Donaldson *et al.* (as shown in Fig. 5c) was tested for impedance at 15 and 103 days of implantation to reflect the stability of the electrode, and the SNR of this electrode showed no significant difference before and after long-term storage. This electrode used transparent PEDOT:PSS as a replacement for silver interconnects within the transparency window, achieving electrodes with both good conductivity and transmissivity.[74]

In terms of functionality, PEDOT exhibits good conductivity, transmittance, and biocompatibility, and the schematic diagram of PEDOT deposition is shown in Fig. 6a. As depicted in Fig. 6b, it can be seen that when PEDOT-coated electrodes are implanted in the body (blue), there is a slight increase in impedance.[31] However, in comparison to the bare gold electrode (black), the impedance of the PEDOT-coated electrode experiences a significant decrease. Elisa *et al.* discovered that applying the PEDOT-CNT coating results in an expansion of the effective area of the electrode nanostructure, leading to an

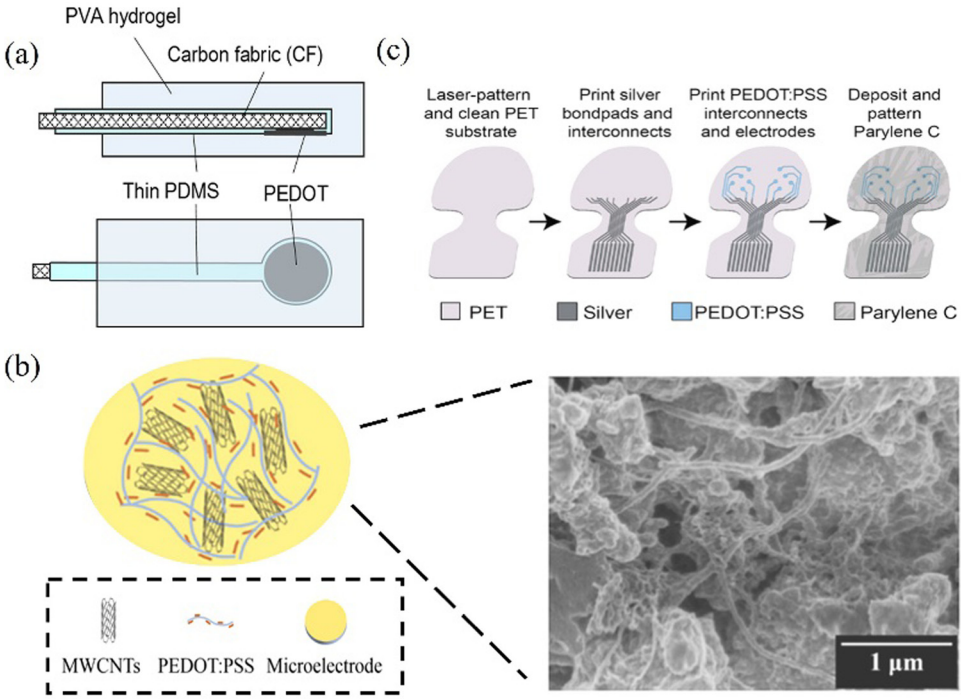

Fig. 5 (a) Based on the cross-section (top) and bottom view of the hydrogel PEDOT-CF ECoG electrode, the PEDOT-CF electrode has low impedance and is good compared to other conductive polymers in chemical stability and electrical performance. Reprinted with permission from ref. 33. Copyright 2018, Scientific Reports. (b) Schematic representation of the electrochemical deposition of MWCNTs and PEDOT:PSS nanocomposites onto microelectrodes. The SEM image of the microelectrode structure is shown on the right. Reprinted with permission from ref. 31. Copyright 2021, American Chemical Society. (c) A structural schematic utilizing PET as a transparent patch material to enhance the transparency of the electrode window. This improvement is achieved through the implementation of PEDOT:PSS interconnects in the window area, enabling contact with inkjet-printed silver interconnects. Reprinted with permission from ref. 74. Copyright 2022, WILEY.

augmentation in the charge exchange between the electrode and the solution. They find that the integral area on the cyclic voltammetry (CV) curve magnifies by a factor of 350, and the enhancement in charge transfer capability becomes more pronounced as the size of the electrode being coated increases.[99] Additionally, the coating of PEDOT:PSS enhances electrical properties and also improves optical properties. Yang *et al.* revealed that due to the PEDOT:PSS coating, there is a slight increase in transmittance. This result makes the PEDOT:PSS polymer advantageous for preparing transparent electrodes.[49]

3.1.2 Polypyrrole. PPy is a common conductive polymer. Research on PPy began in 1989. Machida *et al.* synthesized highly conductive PPy with a conductivity of up to 190 S cm^{-1} in a ferric chloride solution. They found that when $FeCl_2$ was added before the reaction to control the oxidation potential of $FeCl_3$ in a methanol solution, the conductivity of PPy could be increased to a value equivalent to that obtained through electrochemical polymerization (220 S cm^{-1}).[110] This opens up a pathway for the chemical synthesis of highly conductive PPy, providing more options for subsequent work. For example, the electrode prepared by Qi *et al.* consists of a PDMS layer, PPy layer, and PPy nanowires, where the PPy layer is electrochemically polymerized onto the PDMS layer (Fig. 7a) to avoid the delamination of the PPy electrode from the PDMS due to their mismatch in Young's modulus; they fabricated a layer of PPy nanowires on the PPy electrode to enhance their adhesion to the skin, and a comparison of adhesion between before and after modification is shown in Fig. 7b. Rikky *et al.* fabricated a PPy electrode as a control system to release drugs and monitor ECoG signals (Fig. 7c).[8]

Fig. 8a shows the impedance test results of PPy thin-film and Au thin-film electrodes with the same geometric surface area. In comparison, the impedance of PPy films with the same surface area is smaller than 100 Hz. PPy not only has good conductivity but also biocompatibility and is widely used in the preparation of ECoG electrodes. Petr *et al.* proposed that iron(III) chloride is the oxidant of first choice in the preparation of PPy and displays biocompatibility. From long-term experience, they compared the two forms of PPy, salt and alkali, and found that both had lower cytotoxicity, while the alkaline form of PPy had lower cytotoxicity (Fig. 8b).[79] Almira *et al.* pointed out in 2007 that PPy did not cause cytotoxicity in mouse peritoneal cells,[111] making it an attractive material for biomedical applications *in vivo*.[112] For example, PPy can be applied to delivery devices for epilepsy treatment drugs.[8] Although PPy has its advantages, there is currently a problem of decreased conductivity due to peroxidation, which limits its long-term use.[113]

3.2 Structural materials

Ensuring good conformal properties of the electrode upon tissue contact has long been a pursuit in the development of flexible ECoG thin-film electrodes.[114] The flexibility of the sub-

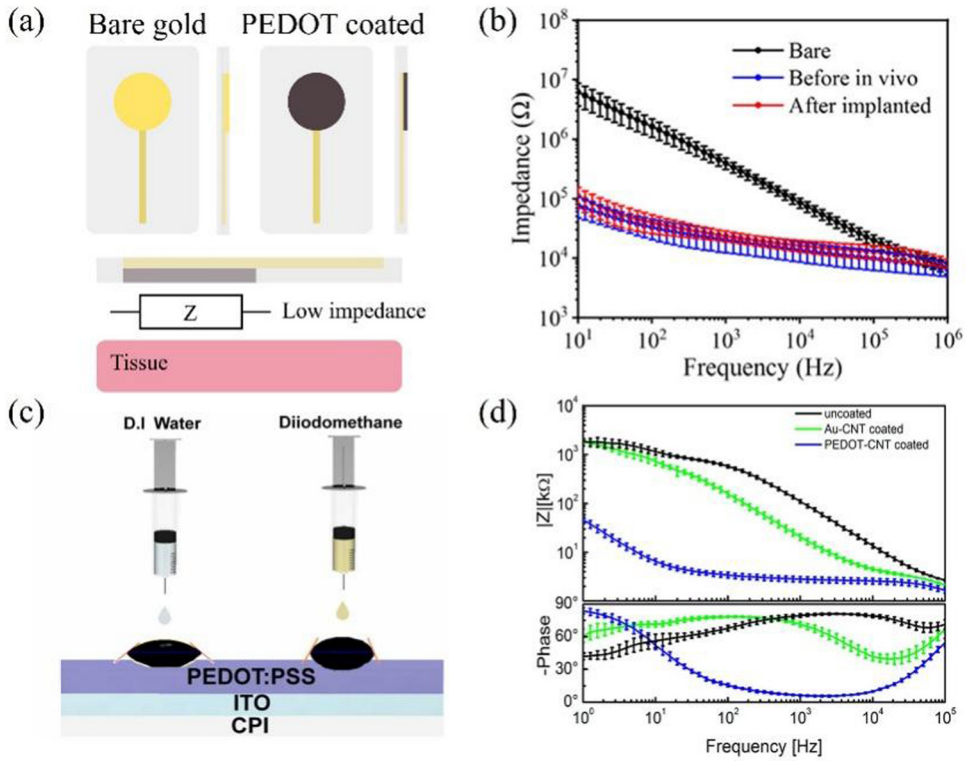

Fig. 6 (a) Schematic of electrodes before and after coating PEDOT. (b) Impedance comparison diagram related to bare (black), before *in vivo* (blue) and after implanted (red). Reprinted with permission from ref. 31. Copyright 2021, American Chemical Society. (c) Measurement of the surface energy of the spin-coated PEDOT:PSS layer for the electrodes using D.I water and diiodomethane. Reprinted with permission from ref. 109. Copyright 2022, Elsevier. (d) Impedance spectra of uncoated (black), gold-CNT-coated (green), and PEDOT-CNT-coated (blue) electrodes (mean and standard deviation of 64 recording sites for each coating). Reprinted with permission from ref. 87. Copyright 2013, American Chemical Society.

strate directly impacts the overall flexibility of the electrode. Commonly employed flexible polymer materials for electrodes encompass PDMS, PI, parylene, and LCP. Over the recent years, the selection of patches for ECoG thin-film electrodes has expanded beyond individual polymer materials, with the emergence of composite structures that combine PDMS and parylene flexible films. This multilayer structure exhibits multiple advantageous properties that collectively enhance its ability to adapt to the intricate brain environment.

3.2.1 Polydimethylsiloxane. PDMS is a silicone-based elastomer[115] which has flexibility,[40,42] processability,[37] biocompatibility,[39,116,117] corrosion resistance[118] and transparency,[31,119] and it is frequently used as substrate materials for flexible electrodes. For example, carbon nanotube arrays (CNTA) can be transported to PDMS through chemical vapor deposition (CVD) to achieve electrode flexibility.[41] Chou *et al.* displayed a significantly curled PDMS electrode.[38] However, the single-layer PDMS substrate has poor adhesion to most metal materials and it is difficult to precipitate metal interconnects on the surface. Therefore, the electrode array, enclosed in a double-layer (DL) PDMS setup for gold interconnects as an insulation layer, shows good biocompatibility.[42] The double-layer membrane structure permits the utilization of materials with distinct functionalities in each layer.[120] In recent years, the adhesion of flexible structures to metal electrode materials has been improved by combining PDMS and parylene materials. In Fig. 9a, a flexible transparent electrode employs PDMS as a pliable substrate, wrapped with Cr/Au electrodes through a parylene interlayer and finally reduced impedance through PEDOT:PSS and MWCNTs material at the contact site between the electrode and the skin. It is considered advantageous that this electrode strategically employs diverse functional polymer materials across distinct structures, resulting in an average impedance of 20.2 ± 7.9 kΩ.[31] Similarly, Ochoa *et al.* chose PDMS (100 ~ 200 μm in thickness) as their flexible structure material and made the ECoG electrode, confirming the conformal coverage of the electrode over a curvature of 1 cm^{-1}.[40] Similarly, Vargo *et al.* fabricated an electrode from PDMS that can stably record ECoG signals.[43]

The performance testing of PDMS focuses on mechanical properties, including finite element analysis,[42] mechanical cycling testing and repeated extrusion testing. Zhao *et al.* fabricated a five-layer gold film structure electrode (green) with PDMS substrate and interlayer connection through Au nanopillars and compared its stretchability with single-layer gold film electrode (black) and double-layer gold film electrode (red) (Fig. 10a and b).[37] The stretchability of the single-layer electrode is 80%, and that for the double-layer electrode is 120%, while the stretchability of the five-layer electrode reached 140%. Importantly, its resistance remained stable even after

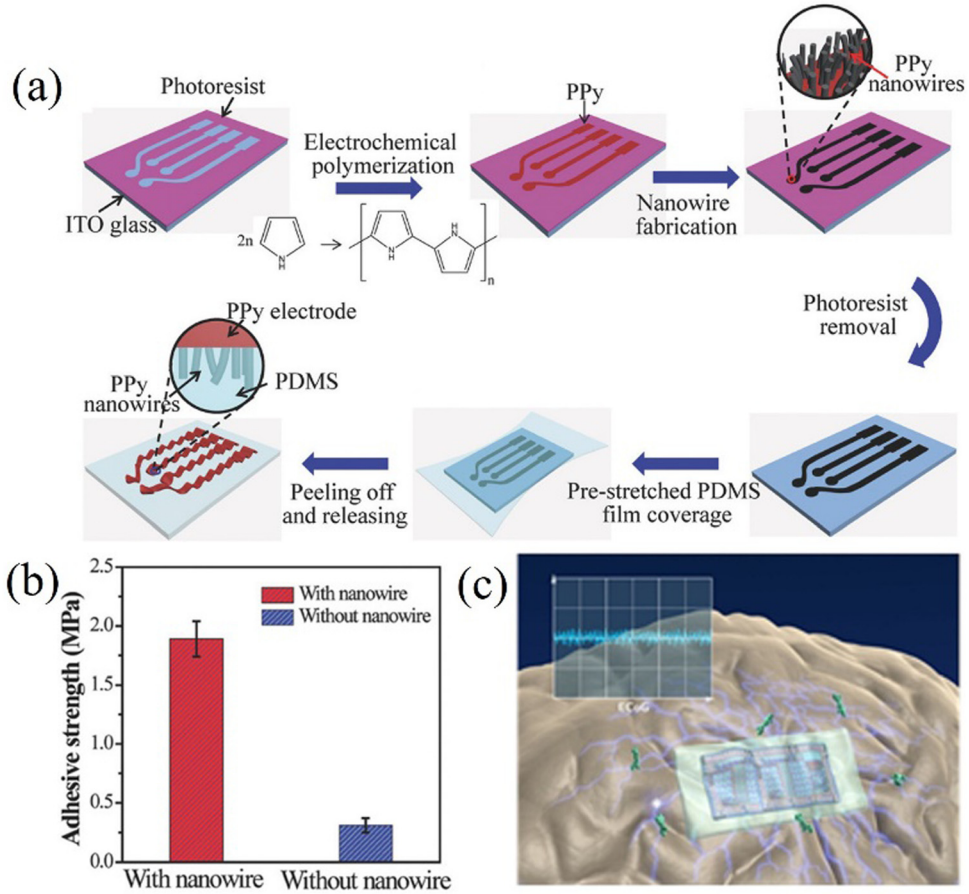

Fig. 7 (a) A preparation method for PPy array electrodes. Reprinted with permission from ref. 95. Copyright 2017, WILEY. (b) Comparison of electrode adhesion before and after PPy nanowires modification. Reprinted with permission from ref. 95. Copyright 2017, WILEY. (c) Schematic diagram of the ECoG drug delivery device for treating epilepsy. Reprinted with permission from ref. 8. Copyright 2016, Elsevier.

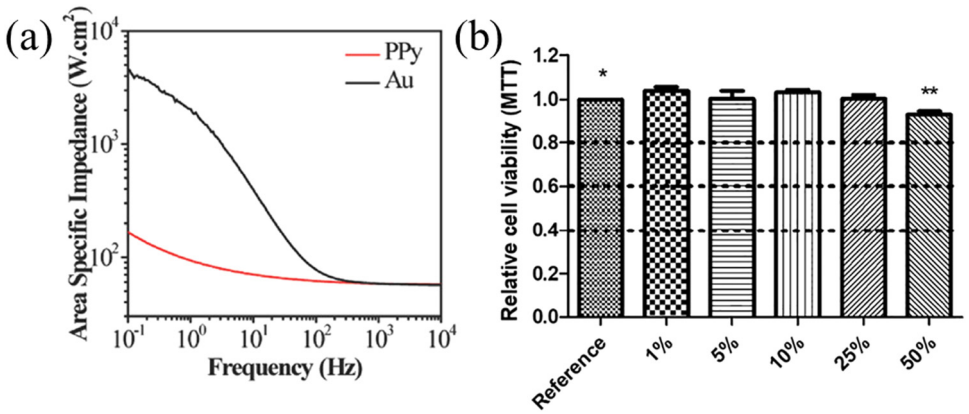

Fig. 8 (a) Impedance compared with the PPy film and Au film. Reprinted with permission from ref. 95. Copyright 2017, WILEY. (b) Cytotoxicity of extracts of PPy towards NIH/3T3 cells compared to the reference. Reprinted with permission from ref. 79. Copyright 2018, Elsevier.

undergoing extensive cyclic testing. Chou *et al.* demonstrated the capability to execute a continuous bending cycle on the thin film, ranging from 0° to 180° and then returning to 0° at a rate of one cycle per second. Additionally, the bending cycles are performed on two distinct electrodes with varying traces, revealing no notable resistance alterations in either of the electrodes.[38] The electrode remains mechanically intact after undergoing 200 000 bending cycles. Li *et al.* used a compression-based technique to measure the average electrode phase change resulting from 100 and 1000 presses, which were $-18.3 \pm 4.9°$ and

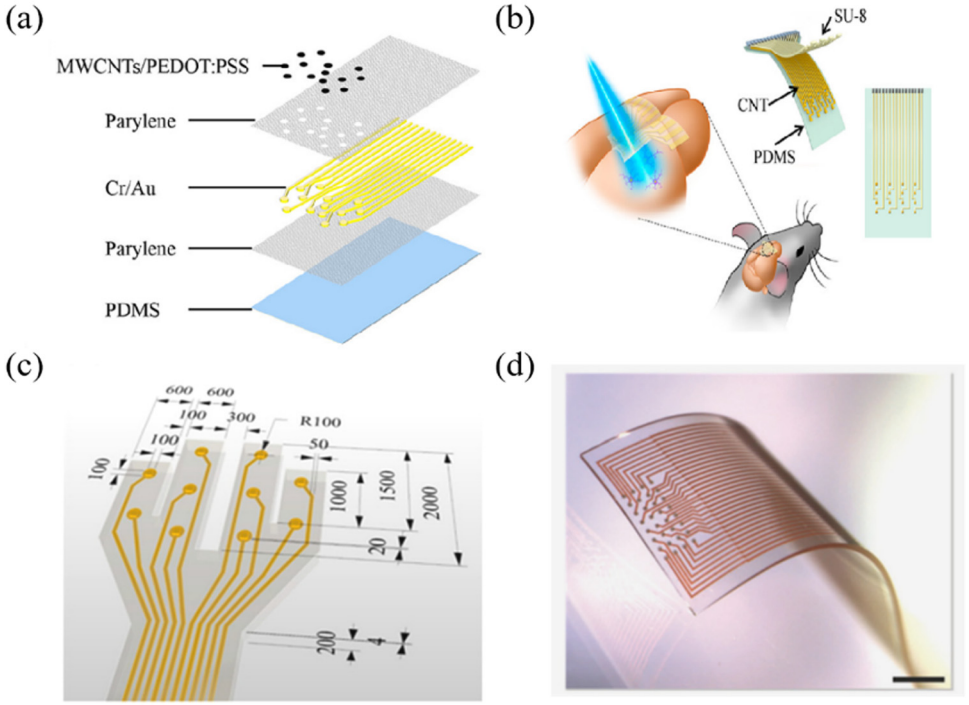

Fig. 9 (a) A schematic of the electrode structure configuration using a two-layer parylene encapsulated metal electrode, PDMS as a flexible substrate and PEDOT:PSS as a contact coating. Reprinted with permission from ref. 31. Copyright 2021, American Chemical Society. (b) Schematics of the stretchable transparent CNT electrode array. Reprinted with permission from ref. 121. Copyright 2018, American Chemical Society. (c) Multichannel ECoG electrode for mixed PDMS-parylene C. Reprinted with permission from ref. 122. Copyright 2022, Elsevier. (d) Stretchable 32 channel electrode on the PDMS substrate (Scale bar, 1 mm). Reprinted with permission from ref. 122. Copyright 2022, Elsevier.

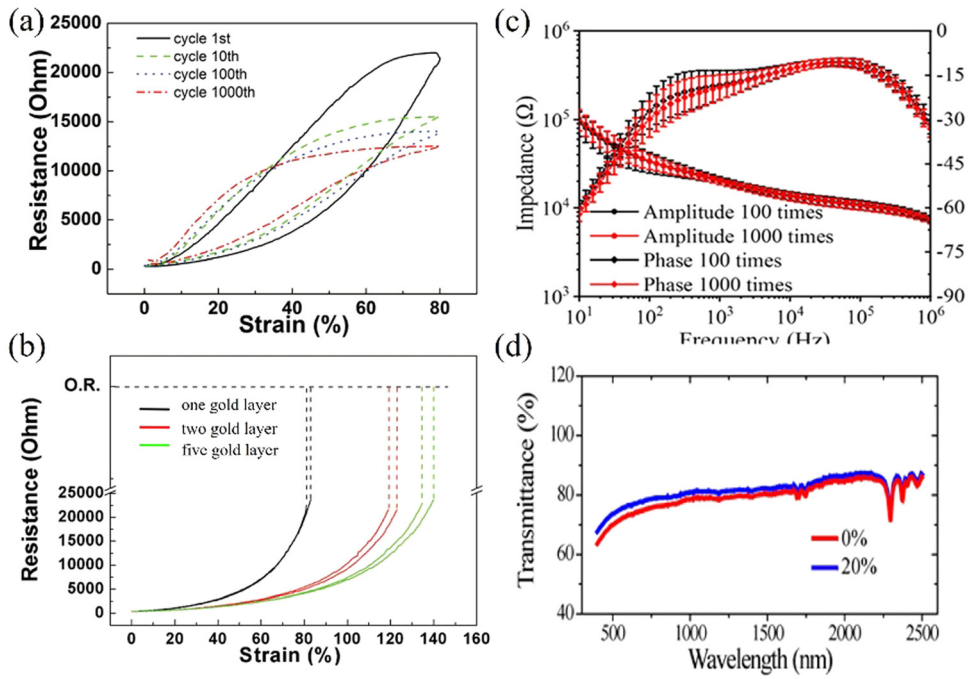

Fig. 10 (a) The stretchability of the five-layer structure electrodes reaching 140% compared to 80% for the original one-layer electrodes and 120% for double-layered electrodes.[37] (b) The resistance–strain curve of the five-layer electrodes after 1, 10, 100, and 1000 stretching cycles, indicating the stability of the electrode after prolonged stretching cycles.[37] (c) Impedance of electrodes after pressing 100 and 1000 times. Reprinted with permission from ref. 31. Copyright 2021, American Chemical Society. (d) Optical transmittance of a CNT/PDMS complex before stretching and under stretching to a strain of 20%. Reprinted with permission from ref. 121. Copyright 2018, American Chemical Society.

−19.1 ± 4.2°, and the impedance values were 20.5 ± 2.1 kΩ and 20.0 ± 1.6 kΩ at 1 Hz (Fig. 10c).[31] Of course, mechanical stretching can also affect the optical properties of thin films. Zhang *et al.* found that at a 20% stretching degree, the transmittance of the CNT/PDMS electrode is higher than that at non-stretching (Fig. 10d).[121]

3.2.2 Parylene. Parylene materials exhibit good metal adhesion, biocompatibility, processability and transparency.[123] Thin films of flexible array patches are frequently fabricated using chemical vapor deposition (CVD),[123] serving as adhesive and protective layers for metal electrodes.[124] The four common parylene variants[125] include parylene C, parylene N, parylene D and parylene HT. Among these, parylene HT stands out with a high-temperature resistance (about 350 °C),[50] facilitating the creation of continuous structures and exhibiting outstanding conformal properties. Transparent electrodes suitable for ECoG signal recording and two-photon Ca^{2+} imaging can be fabricated through the sputter-deposition of ITO.[50] Parylene C has excellent electrical performance and is widely used in commercial electrodes. Fig. 11a shows the flexible ECoG electrode made of parylene C substrate material and demonstrates its good curling flexibility.[55] Parylene not only exhibits good flexibility but also demonstrates biocompatibility, making it a common choice for encapsulating metal electrodes.[38]

In terms of mechanical properties, parylene exhibits a low Young's modulus. Yang *et al.* determined the Young's modulus of a parylene C film through cyclic nanoindentation testing, which remains relatively constant at approximately 4 GPa.[49] As shown in Fig. 12a, Setogawa *et al.* calculated the bending stiffness of the device with and without the metal wiring layer as a function of the parylene thickness. Yamagiwa *et al.* presented the variation of deflection conducted on substrates composed of different thicknesses of parylene N and parylene C composites.[54] As the temperature gradually increases, the deflection of the substrate material continues to increase, displaying the favorable application scenarios of parylene materials in the field of flexible electrode substrates. As shown in Fig. 12b, the resistance went up as the drop spacing increased. However, the growth rate of resistance on parylene is significantly lower than that on PDMS.[126] Moreover, parylene exhibits good electrical and optical properties. Choi *et al.* developed a parylene-based ECoG electrode with an average impedance range of 3.7 kΩ to 1.6 mΩ (1 kHz: 13.9 kΩ) (Fig. 12c).[127] In addition, the parylene electrode sputtered with ITO has a transmittance of 80% in the visible light region of 450–750 nm.[52] Delamination is reported as one of the most common failure mechanisms of thin-film electrodes, and the adhesion force between the electrode and the film determines the lifespan of the electrode.[128] Parylene materials have good adhesion performance in contrast to other polymer films, and peeling is commonly used to validate the adhesion strength of parylene to the electrode material. Nevertheless, this adhesion strength is susceptible to environmental factors. The peeling test was conducted following a 30-minute immersion in PBS, resulting in the detachment of some metals from the parylene film, indicating diminished adhesion of the parylene film to metals in humid conditions.[38] Kim *et al.* compared the silver wire printed on PDMS (blue) and transferred it to a parylene film (red) as a function of drop spacing and conducted lifetime tests on parylene electrodes, revealing the alterations in electrode impedance and channel count, as depicted in Fig. 12d.[51] Within 13 days, the initial impedance increased from 14.2 kΩ to 40 kΩ (n = 16), and after 13 days, the impedance of the electrode significantly decreased.

3.2.3 Polyimide. PI material exhibits good biocompatibility, thermal stability, dynamic tensile strength and structural

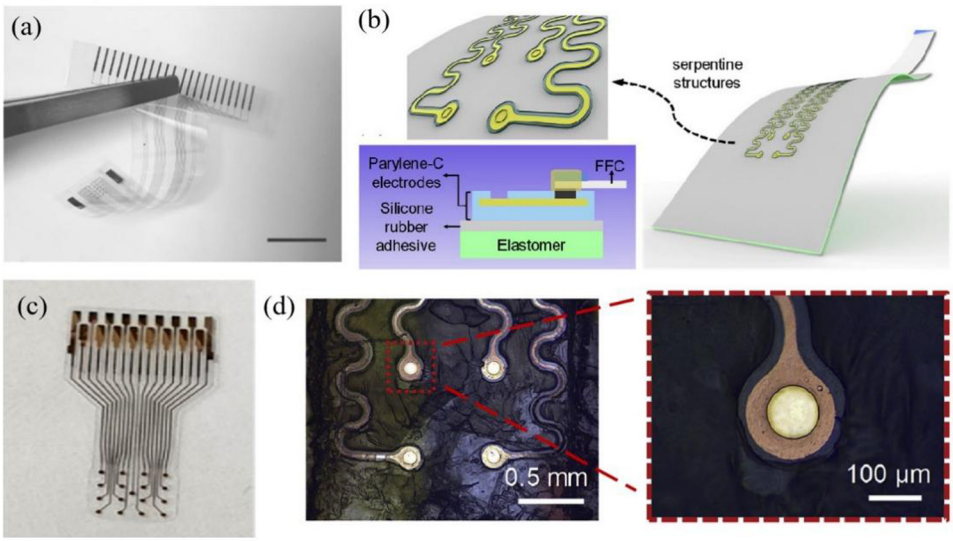

Fig. 11 (a) The flexibility of an ECoG electrode prepared using parylene C as a substrate. Reprinted with permission from ref. 55. Copyright 2022, MDPI. (c) A parylene C coated electrode that has been stable for up to 56 days (equivalent to 115 days) in life testing. Reprinted with permission from ref. 51. Copyright 2022, Elsevier. (b and d) Schematic diagram and micrograph of a serpentine structure. (left 0.5 mm, right 100 μm) Reprinted with permission from ref. 32. Copyright 2019, Elsevier.

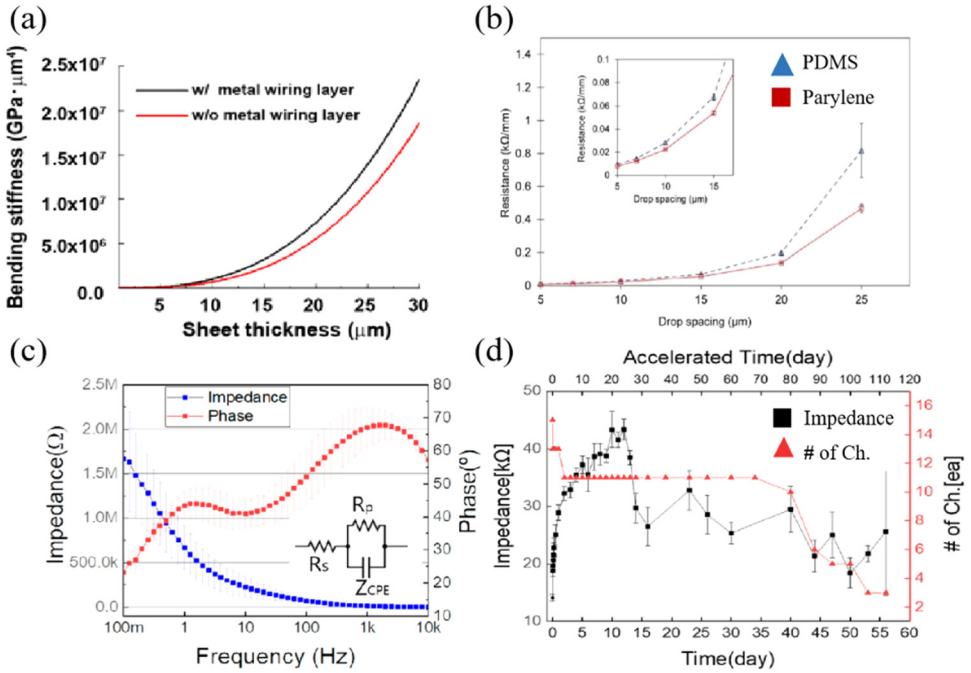

Fig. 12 (a) Calculated bending stiffness of the device with and without the metal wiring layer as a function of the parylene thickness. Reprinted with permission from ref. 129. Copyright 2023, BMC. (b) Comparison of resistance between the two electrode preparation methods. Reprinted with permission from ref. 126. Copyright 2017, Elsevier. (c) Impedance and phase plots for the fabricated parylene C-based ECoG electrodes. Reprinted with permission from ref. 127. Copyright 2020, MDPI. (d) Plot shows the impedance variation and the number of alive channels during the lifetime test, reflecting the stability of the structure. Reprinted with permission from ref. 51. Copyright 2022, Elsevier.

integrity.[115] It is suitable for insulation layers in integrated circuits, active electronic devices and bioelectrodes through spin coating (Fig. 13a).[34] Furthermore, PI displays good air permeability, which can prevent skin inflammation caused by long-term records. The primary role of the PI film is to passivate and protect the electrode structure. Fig. 13b displays the manufacturing diagram of a 32-channel conformal PI electrode, and this electrode can conform to the curvature of the tissue and perfectly adhere to brain. Similarly, Fig. 13c shows an insulating layer situated above the electrode, fabricated through the combination of capacitive $BaTiO_3$ and PI, with the resultant leakage current from this structure measuring only a few nanoamps.[67] The flexible gold film electrode is a sandwich structure made of 5 μm PI.[98] PI material exhibits a certain flexibility. Vomero *et al.* manufactured a highly stable multi-layer thin-film electrode, which is displayed by folding the 12-electrode glassy carbon array onto the PI substrate,[72] and there is no significant change in impedance of this electrode before and after *in vivo* and *in vitro* testing. In comparison to other flexible materials, PI materials exhibit greater durability. Tolstosheeva *et al.* designed a flex-rigid ECoG electrode, and they chose PI as the substrate because it was considered to have better robustness at the same thickness.[130] Four years later, they prepared an ECoG electrode with waterproof properties that could maintain impedance stability in saltwater for 140 days (Fig. 13d).[70]

PI is being focused on in terms of mechanical properties, and Lin *et al.* investigated the alteration in conductor path resistance of the PI electrode under mechanical strain prior to fracture.[131] The electrode resistance exhibited an almost linear increase with the rising applied mechanical strain, and the tensile performance reached a threshold of 10%, which is sufficient for implantation applications. Xu *et al.* measured the stress–strain curve and deformation force curve for PI films with thicknesses of 4 μm, 8 μm, 23 μm, and 50 μm. When the Young's modulus is similar, an increase in the thickness of the PI film leads to a corresponding rise in the ultimate tensile strength of the film.[132] When the electrode is placed in the brain environment, the stability of the electrode in the humoral environment and the conformability of the test determine the signal quality of the electrode. Tolstosheeva *et al.* compared the impedance changes of long-cured PI, short-cured PI and parylene in 170 days of body fluid testing and found that long-term cured PI has good impedance stability and is suitable as a high waterproof barrier (Fig. 14a shows changes in impedance of long-cured PI). In Fig. 14b, a Comsol model was employed to test the stress distribution in a PI electrode with dimensions of 4 μm, 10 μm and 20 μm within the cerebral cortex of rats (with L0 representing the working area where the electrode contacts the cortex, and L1 indicating the opposite end of the electrode), the force required for 10 μm electrode to fit the brain is much smaller than that required for a 20 μm electrode. The miniaturization and lightweight development of the electrode can reduce the harm it brings to the subject.[23] In terms of optical performance, Zátonyi *et al.* measured the optical transmission spectrum of PI/ITO/PI ECoG electrodes across wavelengths ranging from 400 nm to 720 nm. The transmittance

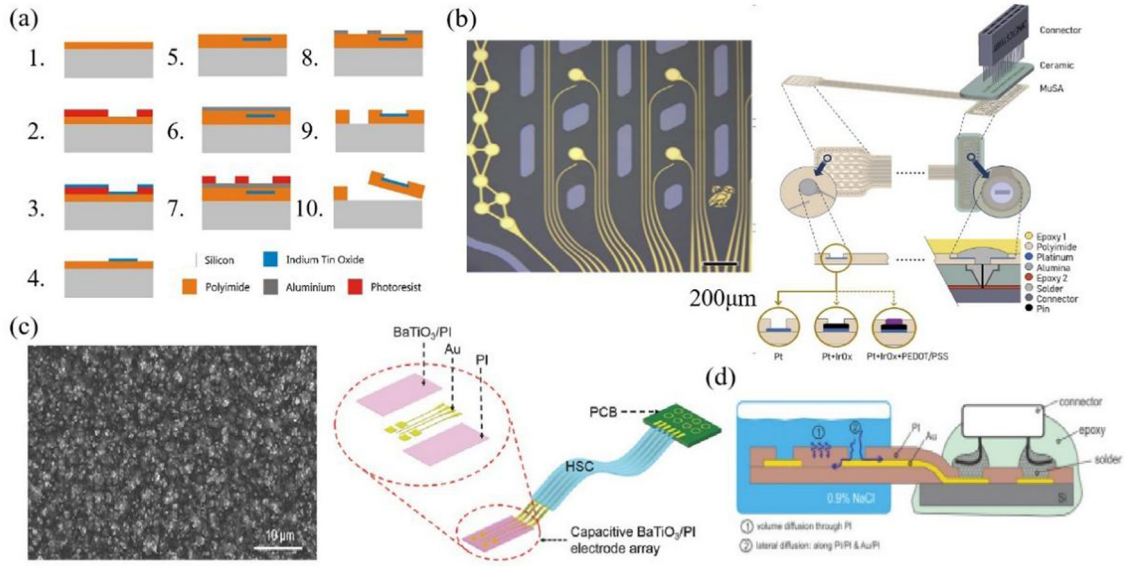

Fig. 13 (a) Schematic of electrode preparation using PI as substrate. Reprinted with permission from ref. 34. Copyright 2018, Elsevier. (b) The manufacturing diagram is about a 32-channel conformal PI electrode that can better fit the surface of the brain and bring the electrode closer to the signal source. The left image depicts the microscopic view of the electrode area, measuring 200 μm. Reprinted with permission from ref. 23. Copyright 2017, Elsevier. (c) Electrode array created by integrating capacitive $BaTiO_3$ and PI, with PI serving as an insulating protective layer. (The left image shows the SEM image of the prepared $BaTiO_3$/PI composite film, measuring 10 μm) Reprinted with permission from ref. 67. Copyright 2017, WILEY. (d) The electrodes encapsulated with PI are immersed in salt water, reflecting the good waterproof properties of PI. Reprinted with permission from ref. 70. Copyright 2015, Elsevier.

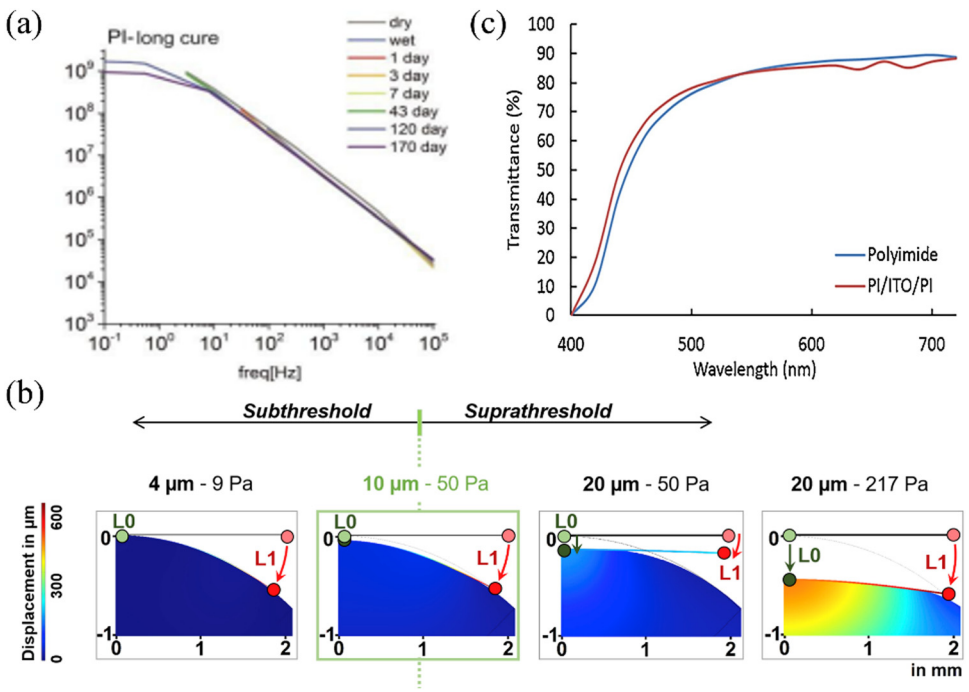

Fig. 14 (a) Long term cured BPDA-PPD PI electrodes maintain stable impedance during long-term testing. Reprinted with permission from ref. 70. Copyright 2015, Elsevier. (b) Finite element analysis images of electrodes with varying thicknesses under diverse forces on the cerebral cortex surface. Reprinted with permission from ref. 23. Copyright 2020, Elsevier. (c) the transmittance of PI/ITO/PI ECoG electrodes. Reprinted with permission from ref. 34. Copyright 2018, Elsevier.

throughout the entire wavelength range consistently remained at approximately 80% (Fig. 14c), and this reflects the good transmittance of PI.[34]

3.2.4 Liquid crystal polymer. The molecular chains of liquid crystal polymers (LCP) exhibit a one-dimensional and two-dimensional long-range ordered arrangement in structure,

exhibiting good flexibility, fluidity,[60] orientation and low water permeability. These characteristics are advantageous for prolonging the reliability and lifespan of implanted arrays. Moreover, LCP serves as a self-adhesive thermoplastic material, facilitating the integration of multi-layer structures in thin-film electrodes.[133]

Fig. 15a shows a design of the LCP electrode. Based on the improvement of electrode size, Chiang *et al.* designed five LCP thin-film electrodes based on thin-film technology, and these electrodes can be applied to collect ECoG signals from rodents, non-human primates and humans according to different application scenarios.[133] Fig. 15b shows the 25-channel neural electrodes with an LCP substrate. Woods *et al.* compared the electrode lifespans of LCP and PI, illustrating that the LCP-encapsulated gold electrode outperforms the PI-encapsulated gold electrode in terms of longevity.[134] By predicting accelerated aging results, the device can maintain integrity for over 3.4 years. Using mechanical property testing, Chiang *et al.* compared and analyzed the maximum bending force that commercial and LCP thin-film electrodes may exert on the brain from the four-point bending test and brain geometry analysis.[133] Nicholas *et al.* calculated the effective flexural modulus of LCP film, LCP thin-film ECoG array, silicon, the bending force of silicon-covered LCP, and commercial electrode. Then, they estimated the maximum force these components could exert on the human brain and found that the LCP thin film has a maximum pressure on the human brain that is only higher than the LCP film, and the Young's modulus is within 10^{-1} GPa.[59] Michael *et al.* tested the biocompatibility of the LCP electrode. After 3 days and 28 days of recording, a comparison with the electrode experimental group revealed increased glial fibrillary acidic protein reactivity of astrocytes in the control group, whereas a minimal increase was observed in astrocyte activation in the electrode experimental group, indicating the favorable biocompatibility of the LCP electrode.[135]

4. Summary and outlook

The polymer materials have been extensively used for ECoG thin-film electrodes. Polymers such as PDMS provide flexibility to the structure of ECoG thin-film electrodes, while polymers such as PEDOT possess good conductivity to the ECoG thin-film electrodes. To enhance the electrical properties of polymers, the focus is now on minimizing impedance between brain tissue and electrodes. The application of conductive polymer coatings can further reduce the impedance compared to the uncoated electrodes. In terms of mechanical properties, flexible polymer materials have Young's modulus more similar to the brain tissue, providing greater comfort and less damage when placing the electrodes and making them easier to conform to the cerebral cortex. On this basis, the light transmittance of polymer materials can also provide a pathway for artificial regulation of brain activity through light stimulation. These aspects collectively underscore the merits of polymer-based ECoG thin-film electrodes.

However, the focus of ECoG thin-film electrodes is on detecting high-quality signals and avoiding secondary damage. On the one hand, many polymer materials for electrodes are used to reduce damage to the brain tissue. On the other hand, subjecting individuals to craniotomies to remove the electrode after rescue or experiments can cause significant damage. If electrode materials could be engineered to undergo controlled

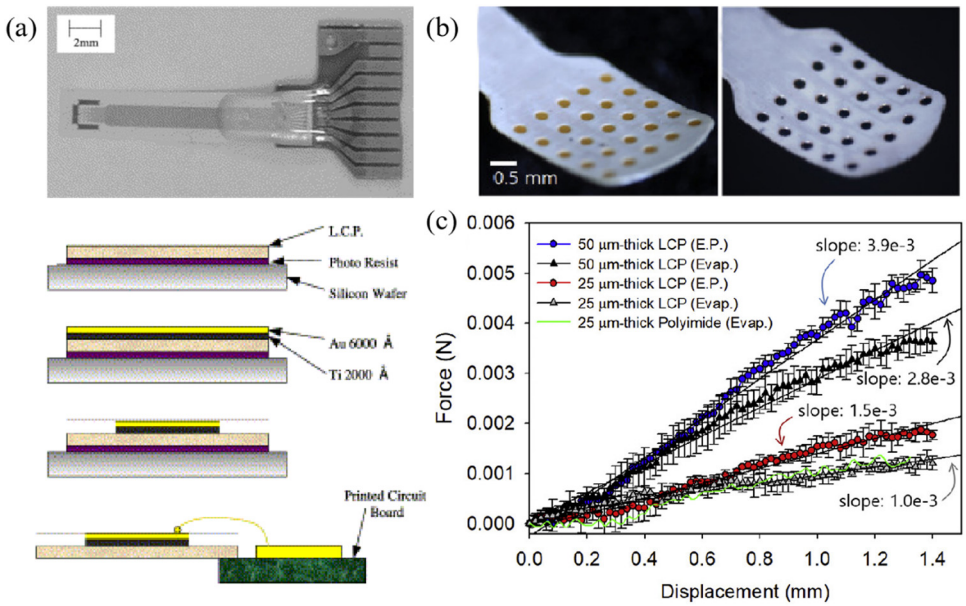

Fig. 15 (a) The schematic and the fabrication process of the LCP electrode. Reprinted with permission from ref. 136. Copyright 2004, Elsevier. (b) 25 channel neural electrode electroplated gold (left) or iridium oxide (right) based on LCP. Reprinted with permission from ref. 137. Copyright 2019, Elsevier. (c) Bending force for LCP electrodes for electroplating (E.P.) and evaporation (Evap.), as well as flexibility comparison with PI electrodes. Reprinted with permission from ref. 137. Copyright 2019, Elsevier.

degradation within tissue, the adverse effects of repetitive craniotomies could be averted. However, most currently available conductive polymers are not degradable. Natural polymers derived from organic sources present new perspectives; these materials exhibit good flexibility and biocompatibility and can even be safely dissolved or absorbed by the body.[138,139] Chitosan, for instance, offers antimicrobial properties and modifiable conductivity; collagen provides a flexible and biocompatible matrix, while silk fibroin allows for tunable degradation rates. These polymers hold promise as potential materials for the next generation of ECoG thin-film electrodes. Furthermore, subjects often experience restricted mobility caused by the constraints of electrical wires connected to electrodes in long-term experiments with traditional ECoG electrodes.[140,141] Wireless telemetry technology has brought about innovative solutions. By incorporating wireless telemetry modules onto thin films through strategic layering of various components, subjects can enjoy more freedom of movement during experiments. Despite numerous challenges, ECoG thin-film electrodes made of polymer materials continue to be widely utilized due to their exceptional properties.

Data availability

No primary research results, software or code has been included, and no new data were generated or analysed as part of this review.

Conflicts of interest

The authors declare no conflict of interest.

Acknowledgements

This review was supported by the National Natural Science Foundation of China (52203309, 52373240), the Shanghai Sailing Program (22YF1400400), the Shanghai Rising-Star Program (23QA1400100), the Fundamental Research Funds for the Central Universities (2232022D-09), and the Open Fund of State Key Laboratory of Biobased Fiber Manufacturing Technology (SKL202317), Key-Area Research and Development Program of Guangdong Province (2023B0303030002). L. Y. acknowledges the financial support from the Shenzhen Science and Technology Program (Grant No. RCBS20221008093340100) and the funding support of No. SE3Z007 and 52293425. S. S. acknowledges support from the RGC Postdoctoral Fellowship Scheme (P0052633).

References

1 N. Wu, S. Wan, S. Su, H. Huang, G. Dou and L. Sun, *InfoMat*, 2021, **3**, 1174.
2 X. Wang, X. Sun, D. Gan, M. Soubrier, H.-Y. Chiang, L. Yan, Y. Li, J. Li, S. Yu, Y. Xia, K. Wang, Q. Qin, X. Jiang, L. Han, T. Pan, C. Xie and X. Lu, *Matter*, 2022, **5**, 1204.
3 L. Wang, S. Liu, W. Zhao, J. Li, H. Zeng, S. Kang, X. Sheng, L. Wang, Y. Fan and L. Yin, *Adv. Healthcare Mater.*, 2024, 2303316n/a.
4 A. Yu, M. Zhu, C. Chen, Y. Li, H. Cui, S. Liu and Q. Zhao, *Adv. Healthcare Mater.*, 2024, **13**, 2302460.
5 N.-I. Kim, J. Chen, W. Wang, J. Y. Kim, M.-K. Kwon, M. Moradnia, S. Pouladi and J.-H. Ryou, *Adv. Healthcare Mater.*, 2024, 2303581n/a.
6 H. Liu, X. Yuan, T. Liu, W. Zhang, H. Dong and Z. Chu, *Adv. Healthcare Mater.*, 2024, 2304355n/a.
7 X. Wang, X. Xiao, Z. Feng, Y. Wu, J. Yang and J. Chen, *Adv. Healthcare Mater.*, 2023, 2303479n/a.
8 R. Muller, Z. Yue, S. Ahmadi, W. Ng, W. M. Grosse, M. J. Cook, G. G. Wallace and S. E. Moulton, *Sens. Actuators, B*, 2016, **236**, 732.
9 R. Balint, N. J. Cassidy and S. H. Cartmell, *Acta Biomater.*, 2014, **10**, 2341.
10 I. Tubia, M. Mujika, J. Artieda, M. Valencia and S. Arana, *Sens. Actuators, A*, 2016, **251**, 241.
11 G. Chen, D. Dang, C. Zhang, L. Qin, T. Yan, W. Wang and W. Liang, *Soft Matter*, 2024, **20**, 7993.
12 L. Sifringer, L. De Windt, S. Bernhard, G. Amos, B. Clément, J. Duru, M. W. Tibbitt and C. M. Tringides, *J. Mater. Chem. B*, 2024, **12**, 10272.
13 H. Dawit, Y. Zhao, J. Wang and R. Pei, *Biomater. Sci.*, 2024, **12**, 2786.
14 M. E. E. Alahi, Y. Liu, Z. Xu, H. Wang, T. Wu and S. C. Mukhopadhyay, *Mater. Today Commun.*, 2021, **29**, 102853.
15 Q. Zeng and Z. Huang, *Adv. Funct. Mater.*, 2023, **33**, 2301223.
16 D. H. Szarowski, M. D. Andersen, S. Retterer, A. J. Spence, M. Isaacson, H. G. Craighead, J. N. Turner and W. Shain, *Brain Res.*, 2003, **983**, 23.
17 M. Jorfi, J. L. Skousen, C. Weder and J. R. Capadona, *J. Neural Eng.*, 2015, **12**, 011001.
18 H. Wunderlich and K. L. Kozielski, *Curr. Opin. Biotechnol*, 2021, **72**, 29.
19 J. Wang, T. He and C. Lee, *Nano Energy*, 2019, **65**, 104039.
20 N. Sharafkhani, A. Z. Kouzani, S. D. Adams, J. M. Long, G. Lissorgues, L. Rousseau and J. O. Orwa, *J. Neurosci. Methods*, 2022, **365**, 109388.
21 G. Buzsáki, C. A. Anastassiou and C. Koch, *Nat. Rev. Neurosci.*, 2012, **13**, 407.
22 Y. Shi, R. Liu, L. He, H. Feng, Y. Li and Z. Li, *Smart Mater. Med.*, 2020, **1**, 131.
23 M. Vomero, M. F. Porto Cruz, E. Zucchini, F. Ciarpella, E. Delfino, S. Carli, C. Boehler, M. Asplund, D. Ricci, L. Fadiga and T. Stieglitz, *Biomaterials*, 2020, **255**, 120178.
24 G. He, X. Dong and M. Qi, *Mater. Res. Express*, 2020, **7**, 102001.
25 A. Zatonyi, F. Fedor, Z. Borhegyi and Z. Fekete, *J. Neural Eng.*, 2018, **15**, 054003.
26 M. McDonald, D. Sebinger, L. Brauns, L. Gonzalez-Cano, Y. Menuchin-Lasowski, M. Mierzejewski, O.-E. Psathaki, A. Stumpf, J. Wickham, T. Rauen, H. Schöler and P. D. Jones, *Biosens. Bioelectron.*, 2023, **228**, 115223.

27 X. Wei, L. Luan, Z. Zhao, X. Li, H. Zhu, O. Potnis and C. Xie, *Adv. Sci.*, 2018, **5**, 1700625.
28 A. B. Rapeaux and T. G. Constandinou, *Curr. Opin. Biotechnol*, 2021, **72**, 102.
29 C. Rinoldi, Y. Ziai, S. S. Zargarian, P. Nakielski, K. Zembrzycki, M. A. Haghighat Bayan, A. B. Zakrzewska, R. Fiorelli, M. Lanzi, A. Kostrzewska-Księżyk, R. Czajkowski, E. Kublik, L. Kaczmarek and F. Pierini, *ACS Appl. Mater. Interfaces*, 2023, **15**, 6283.
30 X. Wang, M. Wang, H. Sheng, L. Zhu, J. Zhu, H. Zhang, Y. Liu, L. Zhan, X. Wang, J. Zhang, X. Wu, Z. Suo, W. Xi and H. Wang, *Biomaterials*, 2022, **281**, 121352.
31 X. Li, Y. Song, G. Xiao, E. He, J. Xie, Y. Dai, Y. Xing, Y. Wang, Y. Wang, S. Xu, M. Wang, T. H. Tao and X. Cai, *ACS Appl. Bio Mater.*, 2021, **4**, 8013.
32 B. Ji, Z. Xie, W. Hong, C. Jiang, Z. Guo, L. Wang, X. Wang, B. Yang and J. Liu, *J. Materiomics*, 2020, **6**, 330.
33 S. Oribe, S. Yoshida, S. Kusama, S.-I. Osawa, A. Nakagawa, M. Iwasaki, T. Tominaga and M. Nishizawa, *Sci. Rep.*, 2019, **9**, 13379.
34 A. Zátonyi, Z. Borhegyi, M. Srivastava, D. Cserpán, Z. Somogyvári, Z. Kisvárday and Z. Fekete, *Sens. Actuators, B*, 2018, **273**, 519.
35 S. Dong, W. Chen, X. Wang, S. Zhang, K. Xu and X. Zheng, *Vacuum*, 2017, **140**, 96.
36 W. Chen, J. Lin, Z. Ye, X. Wang, J. Shen and B. Wang, *Mater. Horiz.*, 2024, DOI: **10.1039/D4MH00753K**.
37 Y. Zhao, C. Li, M. Yu and Z. Yu, *APL Mater.*, 2019, **7**, 101104.
38 N. Chou, S. Yoo and S. Kim, *IEEE Trans. Neural Syst. Rehabil. Eng.*, 2013, **21**, 544.
39 A. Blau, A. Murr, S. Wolff, E. Sernagor, P. Medini, G. Iurilli, C. Ziegler and F. Benfenati, *Biomaterials*, 2011, **32**, 1778.
40 M. Ochoa, P. Wei, A. J. Wolley, K. J. Otto and B. Ziaie, *Biomed. Microdevices*, 2013, **15**, 437.
41 H. Yang, Z. Qian, J. Wang, J. Feng, C. Tang, L. Wang, Y. Guo, Z. Liu, Y. Yang, K. Zhang, P. Chen, X. Sun and H. Peng, *Adv. Funct. Mater.*, 2022, **32**, 2204794.
42 L. Guo, G. S. Guvanasen, X. Liu, C. Tuthill, T. R. Nichols and S. P. DeWeerth, *IEEE Trans. Biomed. Circuits Syst.*, 2013, **7**, 1.
43 S. M. Vargo, T. Belloir, I. Kimukin, Z. Ahmed, D. J. Griggs, N. Stanis, A. Yazdan-Shahmorad and M. Chamanzar, *Presented at 2023 11th International IEEE/EMBS Conference on Neural Engineering (NER)*, 24-27 April 2023, 2023.
44 U.-J. Jeong, J. Lee, N. Chou, K. Kim, H. Shin, U. Chae, H.-Y. Yu and I.-J. Cho, *Lab Chip*, 2021, **21**, 2383.
45 B. Ji, M. Wang, C. Ge, Z. Xie, Z. Guo, W. Hong, X. Gu, L. Wang, Z. Yi, C. Jiang, B. Yang, X. Wang, X. Li, C. Li and J. Liu, *Biosens. Bioelectron.*, 2019, **135**, 181.
46 W. Yang, Q. H. Fan and W. Li, Presented at 2020 IEEE 15th International Conference on Nano/Micro Engineered and Molecular System (NEMS), 27-30 Sept. 2020, 2020.
47 T. J. Richner, S. Thongpang, S. K. Brodnick, A. A. Schendel, R. W. Falk, L. A. Krugner-Higby, R. Pashaie and J. C. Williams, *J. Neural Eng.*, 2014, **11**, 016010.
48 W. R. Lee, C. Im, C. S. Koh, J. M. Kim, H. C. Shin and J. M. Seo, *Presented at 2017 39th Annual International Conference of the IEEE Engineering in Medicine and Biology Society (EMBC)*, 11-15 July 2017, 2017.
49 W. Yang, Y. Gong, C.-Y. Yao, M. Shrestha, Y. Jia, Z. Qiu, Q. H. Fan, A. Weber and W. Li, *Lab Chip*, 2021, **21**, 1096.
50 A. Zatonyi, M. Madarasz, A. Szabo, T. Lorincz, R. Hodovan, B. Rozsa and Z. Fekete, *J. Neural Eng.*, 2020, **17**, 016062.
51 J.-H. Kim, D.-H. Baek, D. H. Kim and D.-W. Park, *Curr. Appl. Phys.*, 2022, **39**, 214.
52 K. Y. Kwon, B. Sirowatka, A. Weber and W. Li, *IEEE Trans. Biomed. Circuits Syst.*, 2013, **7**, 593.
53 F. Vitale, W. Shen, N. Driscoll, J. C. Burrell, A. G. Richardson, O. Adewole, B. Murphy, A. Ananthakrishnan, H. Oh, T. Wang, T. H. Lucas, D. K. Cullen, M. G. Allen and B. Litt, *PLoS One*, 2018, **13**, e0206137.
54 S. Yamagiwa, M. Ishida and T. Kawano, *Ieee, presented at 26th IEEE International Conference on Micro Electro Mechanical Systems (MEMS)*, Taipei, Taiwan, 2013 Jan 20-24, 2013.
55 Y. Kim, S. Alimperti, P. Choi and M. Noh, *Sensors*, 2022, **22**, 1277.
56 S. Shi, Y. Si, Y. Han, T. Wu, M. I. Iqbal, B. Fei, R. K. Y. Li, J. Hu and J. Qu, *Adv. Mater.*, 2022, **34**, 2107938.
57 Y. Si, S. Shi and J. Hu, *Nano Today*, 2023, **48**, 101723.
58 Z. Yang, J. Zeng, Z. Yang, Y. Tong, Y. Lai and X. Cao, *Polymer*, 2022, **255**, 125144.
59 N. S. Witham, C. F. Reiche, T. Odell, K. Barth, C.-H. Chiang, C. Wang, A. Dubey, K. Wingel, S. Devore, D. Friedman, B. Pesaran, J. Viventi and F. Solzbacher, *J. Neural Eng.*, 2022, **19**, 046041.
60 R. Rihani, N. Tasnim, M. Javed, J. O. Usoro, T. M. D'Souza, T. H. Ware and J. J. Pancrazio, *Neuromodulation*, 2022, **25**, 1259.
61 L. Luan, J. T. Robinson, B. Aazhang, T. Chi, K. Yang, X. Li, H. Rathore, A. Singer, S. Yellapantula, Y. Fan, Z. Yu and C. Xie, *Neuron*, 2020, **108**, 302.
62 H. Moon, J. Kwon, J. Eun, C. K. Chung, J. S. Kim, N. Chou and S. Kim, *Adv. Mater. Technol.*, 2024, **9**, 2301692.
63 E. Song, J. Li, S. M. Won, W. Bai and J. A. Rogers, *Nat. Mater.*, 2020, **19**, 590.
64 C. Sung, W. Jeon, K. S. Nam, Y. Kim, H. Butt and S. Park, *J. Mater. Chem. B*, 2020, **8**, 6624.
65 Y. Liu, V. R. Feig and Z. Bao, *Adv. Healthcare Mater.*, 2021, **10**, 2001916.
66 I. B. Dimov, M. Moser, G. G. Malliaras and I. McCulloch, *Chem. Rev.*, 2022, **122**, 4356.
67 C. Chen, M. Xue, Y. Wen, G. Yao, Y. Cui, F. Liao, Z. Yan, L. Huang, S. A. Khan, M. Gao, T. Pan, H. Zhang, W. Jing, D. Guo, S. Zhang, H. Yao, X. Zhou, Q. Li, Y. Xia and Y. Lin, *Adv. Healthcare Mater.*, 2017, **6**, 1700305.
68 A. Schander, S. Strokov, H. Stemmann, T. Teßmann, A. K. Kreiter and W. Lang, *IEEE Sens. J.*, 2019, **19**, 820.
69 E. Borda, D. I. Medagoda, M. J. I. A. Leccardi, E. G. Zollinger and D. Ghezzi, *Biomaterials*, 2023, **293**, 121979.
70 E. Tolstosheeva, V. Biefeld and W. Lang, *Proc. Eng.*, 2015, **120**, 36.

71 M. Vomero, E. Zucchini, E. Delfino, C. Gueli, N. C. Mondragon, S. Carli, L. Fadiga and T. Stieglitz, *Materials*, 2018, **11**, 2486.
72 M. Vomero, E. Castagnola, J. S. Ordonez, S. Carli, E. Zucchini, E. Maggiolini, C. Gueli, N. Goshi, L. Fadiga, D. Ricci, S. Kassegne and T. Stieglitz, *Presented at 2017 8th International IEEE/EMBS Conference on Neural Engineering (NER)*, 25-28 May 2017, 2017.
73 S. Carli, M. Bianchi, E. Zucchini, M. Di Lauro, M. Prato, M. Murgia, L. Fadiga and F. Biscarini, *Adv. Healthcare Mater.*, 2019, **8**, 1900765.
74 P. D. Donaldson, Z. S. Navabi, R. E. Carter, S. M. L. Fausner, L. Ghanbari, T. J. Ebner, S. L. Swisher and S. B. Kodandaramaiah, *Adv. Healthcare Mater.*, 2022, **11**, 2200626.
75 E. Castagnola, L. Maiolo, E. Maggiolini, A. Minotti, M. Marrani, F. Maita, A. Pecora, G. N. Angotzi, A. Ansaldo, L. Fadiga, G. Fortunato and D. Ricci, *Presented at 2013 6th International IEEE/EMBS Conference on Neural Engineering (NER)*, 6-8 Nov. 2013, 2013.
76 D. Kumar and R. C. Sharma, *Eur. Polym. J.*, 1998, **34**, 1053.
77 D. Olvera and M. G. Monaghan, *Adv. Drug Delivery Rev.*, 2021, **170**, 396.
78 I. Fratoddi, I. Venditti, C. Cametti and M. V. Russo, *Sens. Actuators, B*, 2015, **220**, 534.
79 P. Humpolíček, V. Kašpárková, J. Pacherník, J. Stejskal, P. Bober, Z. Capáková, K. A. Radaszkiewicz, I. Junkar and M. Lehocký, *Mater. Sci. Eng. C*, 2018, **91**, 303.
80 S. Bhadra, D. Khastgir, N. K. Singha and J. H. Lee, *Prog. Polym. Sci.*, 2009, **34**, 783.
81 E. M. Geniès, A. Boyle, M. Lapkowski and C. Tsintavis, *Synth. Met.*, 1990, **36**, 139.
82 M. A. Bhat, R. A. Rather and A. H. Shalla, *Synth. Met.*, 2021, **273**, 116709.
83 K. R. Ryan, M. P. Down, N. J. Hurst, E. M. Keefe and C. E. Banks, *eScience*, 2022, **2**, 365.
84 L. Ouyang, C. Musumeci, M. J. Jafari, T. Ederth and O. Inganäs, *ACS Appl. Mater. Interfaces*, 2015, **7**, 19764.
85 H. Aghazadeh, M. K. Yazdi, A. Kolahi, M. Yekani, P. Zarrintaj, J. D. Ramsey, M. R. Ganjali, F. J. Stadler, M. R. Saeb and M. Mozafari, *Curr. Appl. Phys.*, 2021, **27**, 43.
86 S. Manouchehri, B. Bagheri, S. H. Rad, M. N. Nezhad, Y. C. Kim, O. O. Park, M. Farokhi, M. Jouyandeh, M. R. Ganjali, M. K. Yazdi, P. Zarrintaj and M. R. Saeb, *Prog. Org. Coat.*, 2019, **131**, 389.
87 E. Castagnola, A. Ansaldo, E. Maggiolini, G. N. Angotzi, M. Skrap, D. Ricci and L. Fadiga, *ACS Nano*, 2013, **7**, 3887.
88 G. A. Woods, N. J. Rommelfanger and G. Hong, *Matter*, 2020, **3**, 1087.
89 S.-H. Sunwoo, S. I. Han, H. Joo, G. D. Cha, D. Kim, S. H. Choi, T. Hyeon and D.-H. Kim, *Matter*, 2020, **3**, 1923.
90 E. S. Boyden, F. Zhang, E. Bamberg, G. Nagel and K. Deisseroth, *Nat. Neurosci.*, 2005, **8**, 1263.
91 Y. U. Cho, S. L. Lim, J.-H. Hong and K. J. Yu, *npj Flexible Electron.*, 2022, **6**, 53.
92 A. Yazdan-Shahmorad, C. Diaz-Botia, T. L. Hanson, V. Kharazia, P. Ledochowitsch, M. M. Maharbiz and P. N. Sabes, *Neuron*, 2016, **89**, 927.
93 T. Araki, F. Yoshida, T. Uemura, Y. Noda, S. Yoshimoto, T. Kaiju, T. Suzuki, H. Hamanaka, K. Baba, H. Hayakawa, T. Yabumoto, H. Mochizuki, S. Kobayashi, M. Tanaka, M. Hirata and T. Sekitani, *Adv. Healthcare Mater.*, 2019, **8**, 1900130.
94 B. Janarthanan, C. Thirunavukkarasu, S. Maruthamuthu, M. A. Manthrammel, M. Shkir, S. AlFaify, M. Selvakumar, V. R. M. Reddy and C. Park, *J. Mol. Struct.*, 2021, **1241**, 130606.
95 D. Qi, Z. Liu, Y. Liu, Y. Jiang, W. R. Leow, M. Pal, S. Pan, H. Yang, Y. Wang, X. Zhang, J. Yu, B. Li, Z. Yu, W. Wang and X. Chen, *Adv. Mater.*, 2017, **29**, 1702800.
96 M. J. Donahue, A. Sanchez-Sanchez, S. Inal, J. Qu, R. M. Owens, D. Mecerreyes, G. G. Malliaras and D. C. Martin, *Mater. Sci. Eng., R*, 2020, **140**, 100546.
97 N. Rossetti, J. E. Hagler, P. Kateb and F. Cicoira, *J. Mater. Chem. C*, 2021, **9**, 7243.
98 S. Strokov, A. Schander, H. Stemmann, T. TeBmann, W. Lang and A. Kreiter, *Presented at 2017 IEEE SENSORS*, 29 Oct.-1 Nov. 2017, 2017.
99 E. Castagnola, L. Maiolo, E. Maggiolini, A. Minotti, M. Marrani, F. Maita, A. Pecora, G. N. Angotzi, A. Ansaldo, M. Boffini, L. Fadiga, G. Fortunato and D. Ricci, *IEEE Trans. Neural Syst. Rehabil. Eng.*, 2015, **23**, 342.
100 K. Gmucová, *Curr. Opin. Electrochem.*, 2022, **36**, 101117.
101 Z. Song, Y. Ma, A. Morrin, C. Ding and X. Luo, *TrAC, Trends Anal. Chem.*, 2021, **135**, 116155.
102 P. Sakunpongpitiporn, K. Phasuksom, N. Paradee and A. Sirivat, *RSC Adv.*, 2019, **9**, 6363.
103 Y. Hui, C. Bian, S. Xia, J. Tong and J. Wang, *Anal. Chim. Acta*, 2018, **1022**, 1.
104 P. Yadav and A. Patra, *Polym. Chem.*, 2020, **11**, 7275.
105 N. Matsuhisa, X. Chen, Z. Bao and T. Someya, *Chem. Soc. Rev.*, 2019, **48**, 2946.
106 Y. Zhang, C. J. Sheehan, J. Zhai, G. Zou, H. Luo, J. Xiong, Y. T. Zhu and Q. X. Jia, *Adv. Mater.*, 2010, **22**, 3027.
107 N. Nandihalli, C.-J. Liu and T. Mori, *Nano Energy*, 2020, **78**, 105186.
108 Y.-Z. Long, M.-M. Li, C. Gu, M. Wan, J.-L. Duvail, Z. Liu and Z. Fan, *Prog. Polym. Sci.*, 2011, **36**, 1415.
109 V. Raman, J.-E. Lee and H.-K. Kim, *J. Alloys Compd.*, 2022, **903**, 163799.
110 S. Machida, S. Miyata and A. Techagumpuch, *Synth. Met.*, 1989, **31**, 311.
111 A. Ramanaviciene, A. Kausaite, S. Tautkus and A. Ramanavicius, *J. Pharm. Pharmacol.*, 2007, **59**, 311.
112 Y. O. Mezhuev, M. I. Shtil'man and A. A. Artyukhov, *Polym. Sci., Ser. D*, 2021, **14**, 427.
113 I. Gablech and E. D. Głowacki, *Adv. Electron. Mater.*, 2023, **9**, 2300258.
114 T. Cheng, Y. Zhang, W.-Y. Lai and W. Huang, *Adv. Mater.*, 2015, **27**, 3349.

115 M. Xu, D. Obodo and V. K. Yadavalli, *Biosens. Bioelectron.*, 2019, **124–125**, 96.
116 J. Liu, Y. Yao, X. Li and Z. Zhang, *Chem. Eng. J.*, 2021, **408**, 127262.
117 D. Qi, K. Zhang, G. Tian, B. Jiang and Y. Huang, *Adv. Mater.*, 2021, **33**, 2003155.
118 U. Eduok, O. Faye and J. Szpunar, *Prog. Org. Coat.*, 2017, **111**, 124.
119 M. P. Wolf, G. B. Salieb-Beugelaar and P. Hunziker, *Prog. Polym. Sci.*, 2018, **83**, 97.
120 Q.-C. Xia, M.-L. Liu, X.-L. Cao, Y. Wang, W. Xing and S.-P. Sun, *J. Membr. Sci.*, 2018, **562**, 85.
121 J. Zhang, X. Liu, W. Xu, W. Luo, M. Li, F. Chu, L. Xu, A. Cao, J. Guan, S. Tang and X. Duan, *Nano Lett.*, 2018, **18**, 2903.
122 S. Bhaskara, T. Sakorikar, S. Chatterjee, K. V. Shabari Girishan and H. J. Pandya, *Sens. Bio-Sens. Res.*, 2022, **36**, 100483.
123 M. Golda-Cepa, K. Engvall, M. Hakkarainen and A. Kotarba, *Prog. Org. Coat.*, 2020, **140**, 105493.
124 T. Haggren, A. Shah, A. Autere, J.-P. Kakko, V. Dhaka, M. Kim, T. Huhtio, Z. Sun and H. Lipsanen, *Nano Res.*, 2017, **10**, 2657.
125 Y. X. Kato, I. Saito, H. Takano, K. Mabuchi and T. Hoshino, *Neurosci. Lett.*, 2009, **464**, 26.
126 Y. Kim, J. W. Kim, J. Kim and M. Noh, *Sens. Actuators, B*, 2017, **238**, 862.
127 B.-J. Choi, J.-H. Kim, W.-J. Yang, D.-J. Han, J. Park and D.-W. Park, *Appl. Sci.*, 2020, **10**, 7364.
128 P. Oldroyd and G. G. Malliaras, *Acta Biomater.*, 2022, **139**, 65.
129 S. Setogawa, R. Kanda, S. Tada, T. Hikima, Y. Saitoh, M. Ishikawa, S. Nakada, F. Seki, K. Hikishima, H. Matsumoto, K. Mizuseki, O. Fukayama, M. Osanai, H. Sekiguchi and N. Ohkawa, *Mol. Brain*, 2023, **16**, 38.
130 E. Tolstosheeva, V. Gordillo-González, T. Hertzberg, L. Kempen, I. Michels, A. Kreiter and W. Lang, *Presented at 2011 Annual International Conference of the IEEE Engineering in Medicine and Biology Society*, 30 Aug.-3 Sept. 2011, 2011.
131 J. H. Lin, Y. Wang, X. M. Wu, T. L. Ren and L. T. Liu, *Presented at 2009 2nd International Conference on Biomedical Engineering and Informatics*, 17-19 Oct. 2009, 2009.
132 F. Xu, Z. Zhou, H. Li and T. H. Tao, *Presented at 2021 IEEE 34th International Conference on Micro Electro Mechanical Systems (MEMS)*, 25-29 Jan. 2021, 2021.
133 C.-H. Chiang, C. Wang, K. Barth, S. Rahimpour, M. Trumpis, S. Duraivel, I. Rachinskiy, A. Dubey, K. E. Wingel, M. Wong, N. S. Witham, T. Odell, V. Woods, B. Bent, W. Doyle, D. Friedman, E. Bihler, C. F. Reiche, D. G. Southwell, M. M. Haglund, A. H. Friedman, S. P. Lad, S. Devore, O. Devinsky, F. Solzbacher, B. Pesaran, G. Cogan and J. Viventi, *J. Neural Eng.*, 2021, **18**, 045009.
134 V. Woods, M. Trumpis, B. Bent, K. Palopoli-Trojani, C.-H. Chiang, C. Wang, C. Yu, M. N. Insanally, R. C. Froemke and J. Viventi, *J. Neural Eng.*, 2018, **15**, 066024.
135 M. Schweigmann, L. C. Caudal, G. Stopper, A. Scheller, K. P. Koch and F. Kirchhoff, *Front. Cell. Neurosci.*, 2021, **15**, 720675.
136 C. J. Lee, S. J. Oh, J. K. Song and S. J. Kim, *Mater. Sci. Eng. C*, 2004, **24**, 265.
137 J. Jeong, K. S. Min and S. J. Kim, *Microelectron. Eng.*, 2019, **216**, 111096.
138 B. Basavaraju, S. Nagaraja, A. R. Banagar, C. V. Srinivasa, B. T. Ramesh, D. Ramdan and M. I. Ammarullah, *RSC Adv.*, 2024, **14**, 33332.
139 S. Dehghan-Chenar, H. R. Zare and Z. Mohammadpour, *RSC Adv.*, 2024, **14**, 33301.
140 C. Meng, D. Snizhko, Y. T. Zholudov, W. Zhang, Y. Guan, Y. Tian and G. Xu, *Chem. Commun.*, 2024, **60**, 13546–13549.
141 F. Chen, X. Song, J. Fu, J. Liang, J. Zhou, J. Cai, Y. Zhang, M. Zhu, Y. Ding, J. Jiang, Z. Chen, Y. Qi, Z. Zhou, Q. Huang, Y. Zhang and Z. Zheng, *J. Mater. Chem. A*, 2024, **12**, 30298–30308.